PN-ACC-243
97036
C12-223

FINAL REPORT

Covering the Whole Research Period

Submitted to the Human Capacity Development

Bureau for Global Programs, Field Support and Research

US Agency for International Development

Studies of Atmospheric Chemistry and Air Pollution

Principal Investigator: Professor Yehuda Haas

Department of Physical Chemistry and the Farkas Center for Light Induced Processes

The Hebrew University of Jerusalem, Jerusalem, Israel

Collaborator: Dr. Josef Pola

Institute for Chemical Process Fundamentals

Academy of Science of the Czech Republic

16502 Prague-Suchdol, Czech Republic

Project Number C12-223

Grant Number: HRN-5544-G-00-2078-00

AID Grant Project Officer: Dr. M. Rechcigl

Project Duration: 28.9.92-27.9.97

RECEIVED
JAN 15

Table of Contents

page	
3	Executive Summary
4	Research Objectives
	Methods and results
5	Solid phase reactions
	Gas phase reactions
	Theoretical work
6	Impact, Relevance and Technology Transfer
	Project Activities/ Outputs
	Meetings attended
7	Papers published in peer reviewed journals
8	Project Productivity
9	Future work
	Literature cited

Attachments:

Copies of papers 7 and 8 (Copies of papers 1-6 were provided in previous reports).

Executive Summary

The purpose of the project is to study the reaction of ozone with olefins, a major cause for air pollution. In the project, important contributions towards the understanding of the reactions between ozone and olefins were made, and the laboratory in the Czech Republic became a center for study of this major environmental problem.

The main scientific achievements are as follows:

An in depth study of olefin ozonation was performed in cryogenic matrices and in the gas phase. Particular attention was given to the role of secondary ozonides, reactive species that were previously observed in solution, but their presence in the gas phase (e. g. under atmospheric conditions) was dubious. Unequivocal evidence was provided that these compounds are indeed formed in the gas phase. Some of their subsequent reactions were also studied, leading to the characterization of gas phase products. It was found that the final product distribution is strongly temperature dependent. This fact will have to be included in future work that will attempt to simulate the entire chemical processes involved in ozone-olefin chemistry, during day and night at different latitudes and climate conditions.

The work included also a spectroscopic and kinetic study of the reaction at cryogenic matrices, allowing a more complete spectroscopic characterization of the primary and secondary ozonides than previously possible. Environmental effects on the reactivity of the system were analyzed. They may be of relevance to reactions of ozone in aerosols and on surfaces (such as dust particles).

Theoretical aspects of the reaction were also studied, using quantum chemical methods and computations. They led to a unified view of the reaction for different olefins, and led to predictions that were subsequently verified experimentally.

During the project, the Czech laboratory was equipped with modern instrumentation, making it a leading institute in the field. Techniques and skills developed in the project will continue to be used, and will serve to further study problems related to atmospheric chemistry, as well as other gas phase reactions.

4. Research Objectives

The research objectives, as defined in the proposal, were:

Study the reactions of ozone with olefins (mechanism and product distribution) and its significance to atmospheric chemistry. Develop research and monitoring capabilities in Czechoslovakia.

Specific objectives were:

1. Separate homogeneous and heterogeneous contributions to the overall yield as well as to specific reaction channels.

2. Use matrix isolation techniques to follow the formation and reactions of the primary ozonides.

3. Use laser pyrolysis techniques to initiate the reactions and study products' yields.

4. Establish the mechanism of olefin ozonolysis under atmospheric conditions.

The project was part of an effort to help the Czechoslovak economy to deal with environmental problems that were of low priority before 1990. In the meantime the state was divided, and the project continued in the newly formed Czech Republic. The project helped to upgrade considerably the research capabilities of the Czech group; it was recognized as an important development, as shown for instance by the allocation of supplementary grants by the Grant Agency of the Czech Republic. The project involved a number of people in the Czech Republic, one of whom, Dr. Radek Fajgar, stayed for nearly half a year in the Jerusalem and became thoroughly acquainted with novel experimental techniques. One of the participants, Dr. Lavrenti Khachatryan, came from Armenia, and will no doubt help in promoting the scientific ideas developed in the project in his home country.

5. Methods and results

The methods used in these projects and the main results were summarized in eight papers that were published or are in the process of being published in peer reviewed journals. These papers describe in great detail the experimental and theoretical methods that were

used, and the results. They are appended to this report, giving the reader a comprehensive and lucid exposition of the methods and achievements. We therefore include in this section a brief description of the main results, with reference to the appropriate publication.

Solid phase reactions:

The ozonation of ethylene, tetramethylethylene and 1-hexene was studied in argon and CO_2 matrices at low temperatures (12-80 K). All three compounds were found to react with ozone in a CO_2 matrix deposited at low temperature, and having an amorphous structure. The reaction was found to start at 26 K, the temperature at which the matrix undergoes a phase transition. In contrast, only tetramethylethylene (TME) was found to react in an argon matrix, the other two compounds remaining inactive towards ozone up to the softening temperature of argon (~40 K). These results were interpreted as indicating that reaction between olefins and ozone is initiated at low temperatures once the two reactants are free to move to the required configuration. This idea is supported by molecular dynamics simulations on the TME reaction. The infrared spectra of the primary ozonide of TME, as well as of the primary and secondary ozonide of 1-hexene are reported, and compared with quantum chemical calculations. (Papers 1 and 7)

Gas phase reactions

The reaction of several olefins with ozone under low and atmospheric pressure conditions in both a static cell and flow conditions was carried out. Unequivocal evidence for the formation of secondary ozonides was established for the first time under these conditions. This proves unequivocally that the Criegee mechanism [Criegee 1957] applies also to the gas phase ozonation of olefins. The effect of temperature was carefully studied, providing data for the important range of -80 C to room temperature. The purely homogeneous gas phase decomposition of some secondary ozonides was studied by laser sensitized methods, establishing the product distribution. (Papers 3, 4, 6 and 8).

Theoretical work

Semiempirical calculations on the reaction addressed the problem of stereospecificity of the O-O splitting in the primary ozonides. The behavior of trans-substituted alkenes was

rationalized, but the stereoselectivity of the cis-substituted ones cannot yet be accounted for at this level of theory. Ab initio methods were extensively used to calculate the structure, energy and vibrational frequencies of several primary and secondary ozonides for the first time. These data are useful in the complete characterization of these important products (papers 2 and 5).

Molecular dynamics simulations were used to discuss the properties and reactivity of olefins trapped together with ozone in solid argon, providing insight as to the causes of different reactivities in different environments. (papers 1 and 7).

6. Impact, Relevance and Technology Transfer

Our explanation of the inactivity of the ethylene-ozone system in solid argon and the much enhanced reactivity in solid CO_2 and xenon (previously noticed by many workers in the field of them but never accounted for) was accepted enthusiastically. The gas phase data were already cited by other leading research groups (see e.g. Neeb 1996) and became an important factor in the analysis of ozonation reactions.

The purchase of modern instrumentation for the Prague laboratory made an enormous impact on its scientific performance. The staff was trained to use these instruments, and a large amount of data has been acquired. This laboratory will surely continue to have an impact on the gas phase chemistry of ozone and other chemicals, and contribute to the expansion of the scientific and technological basis of the Czech Republic. The training of one of the Czech scientists (Dr. Fajgar) in Jerusalem was a most successful project, beneficial to both laboratories. He had the opportunity not only to operate in a state of the art laboratory, but also to acquaint himself with managerial and administrative aspects of Western-type research.

7. Project Activities/ Outputs

7.1 Meetings attended:

1. International Conference on Low temperature Chemistry, ICLC1 in Moscow (September 1994).

2. Gordon Conference on Low Temperature Physics and Chemistry (Plymouth, NH, August 1995).

3. International Conference on Matrix Chemistry and Physics, Spittal, Austria, (July 1997)

7.2 Papers published in peer reviewed journals

1. U. Samuni, R. Fraenkel, Y. Haas, R. Fajgar and J. Pola

Environmental effects in the formation of the primary and secondary ozonides of ethylene at cryogenic temperatures

J. Am. Chem. Soc. 118, 3687-93 (1996)

2. U. Samuni and Y. Haas

An ab-initio study of the normal modes of the primary and secondary ozonides of ethylene

Spectrochim. Acta A52 1479-92 (1996).

3. L. Khachatryan, R. Fajgar, Y. Haas and J. Pola

Laser photo-sensitized homogeneous decomposition of 3,5-dimethyl-1,2,4-trioxolane: the evidence for intermediacy of products of rearrangements

J. Chem. Soc. perkin Trans. 2 1981-4 (1996)

4. R. Fajgar, J. Vitek, Y. Haas and J. Pola

Observation of secondary-2-butene ozonide in the ozonation of trans-2-butene in the gas phase

Tetrahedron Letters, 37 3391-4 (1996)

5. R. Ponec, G. Yuzhakov, Y. Haas and U. Samuni

Theoretical analysis of the mechanism and stereoselectivity of ozonolysis. Evidence for a modified Criegee mechanism

J. Org. Chem. 62 2757-62 (1997)

6. L. Khachatryan,Y. Haas and J. Pola

Laser induced decomposition of 3,5-dimethyl-1,2,4-trioxolane (secondary butene-2- ozonide) in the gas phase:

J. Chem. Soc. perkin Trans. 2 1147-51 (1997)

7. U. Samuni, Y. Haas, R. Fajgar and J. Pola

Matrix effects in the low temperature ozonation of ethylene, teteramethylethylene and 1-hexene

J. Molec. Struct., in press

Paper submitted

8. R. Fajgar, J. Vitek, Y. Haas and J. Pola

Formation of secondary ozonides in the gas phase ozonation of primary and secondary alkenes

Submitted to J. Am. Chem. Soc. December 1997.

8. Project Productivity

The main research objective, namely to study the reactions of ozone with olefins (mechanism and product distribution) was accomplished in full. The related objective, developing research and monitoring capabilities in Czechoslovakia, was also realized for the research part. The know-how to establish and operate monitoring capabilities exists, it is now a matter of national priorities whether it will be used in practice.

The more specific objectives listed in Section 4 were mostly accomplished as can be verified from the published and submitted papers.

The main innovations in the project were:

- The unequivocal detection of secondary ozonides in the gas phase ozonation of olefins.

- The detailed study of secondary ozonides' homogeneous gas phase dissociation, leading to characterization of the reaction products.

- The characterization of the primary and secondary ozonides formed in cryogenic solids, and the role of the matrix in determining their formation.

- The establishment of the general role of a dipole complex in the reaction [Cremer 1991], leading to a universal modification to the classical Criegee mechanism.

9. Future work

The very successful collaboration of the two laboratories culminated in Dr. Pola's last visit to Jerusalem (November 1997), and the completion of two full papers that were submitted for publication. The close relations that were established guarantee further successful collaboration in the future. A possible research field that may be developed is related to modern material research, which is at the moment being separately pursued in the two institutes.

10. Literature cited

Cremer 1991. D. Cremer, E. Kraka, M. L. McKee and T. P. Radhakrishnan, Chem. Phys. Lett. 187 491 (1991).

Criegee 1957. R. Criegee, Rec. Chem. Prog. 18 111 (1957).

Neeb 1996. P. Neeb, O. Horie and K. K. Moortgat, Tetrahedron Letters 37, 9297 (1996).

Formation of Secondary Ozonides in the Gas Phase Ozonation of Primary and Secondary Alkenes

C12-223

R. Fajgar,[†] J. Vítek,[†] Y. Haas,[‡] and J. Pola[†*]

Contribution from the Institute of Chemical Process Fundamentals, The Czech Academy of Sciences, 16502 Prague, Czech Republic, and Department of Physical Chemistry and Farkas Center for Light-Induced Processes, The Hebrew University of Jerusalem, 91904 Jerusalem, Israel

Abstract: The gas-phase ozonation of a series of alkenes $RCH{=}CH_2$ (R = Et, Hex), *trans*-RHC=CHR (R = Me, Et, i-Pr) and $Me_2C{=}CMe_2$ at -40 - 20 °C, and that of ethene $H_2C{=}CH_2$ at -120 - 0 °C at 10^{-4} v/v concentrations in N_2 at atmospheric pressure have been studied. We present for the first time direct evidence for the formation of secondary ozonides (SOZ) which were unequivocally identified by GC/MS and GC/FTIR methods as high-yield products in all instances except $Me_2C{=}CMe_2$. It is shown that the stereoselectivity for conversion of *trans*-RHC=CHR (R = Me, Et, i-Pr) to *trans*-SOZ in the gas phase is similar to that in solution, and that the yields of secondary ozonides from $RHC{=}CH_2$, but not those from RHC=CHR significantly decrease with increasing temperature. This paper therefore confirms the validity of the Criegee mechanism to atmospheric gas-phase conditions.

REC'D ON DSD/B
JAN 1 5

[†]Institute of Chemical Process Fundamentals.

[‡]Hebrew University

Introduction

Gas-phase ozone-alkene reactions have attracted early[1], continuing[2] and recent[3] attention, since simple alkenes are among most abundant hydrocarbons in the urban atmosphere[4] and over tropical forests[5] and the detailed knowledge on their reaction with ozone would help to model the tropospheric chemistry leading to photochemical smog and to characterize the harmful effects[6] of the reaction products on vegetation. Despite to a large number of studies, complete understanding of the mechanism of this complex reaction is still awaiting further effort.

In analogy with the corresponding ozone-alkene solution-phase reactions[7], the gas-phase ozonations of alkenes are believed[8] to be initiated by the formation of primary ozonide (POZ) followed by its unimolecular dissociation into the carbonyl compound (CC) and a carbonyl oxide (COX), often referred to as the Criegee intermediate (CI). Considerable uncertainties persist, however, concerning the next steps, particularly the reactions of the CI intermediates. As shown in the energy level diagram of Figure 1, the CC+COX pair is formed with a large excess of internal energy. In solution (or in a cryogenic matrix) they are rapidly vibrationally relaxed, leading to the formation of secondary ozonides (SOZ), the latter being easily isolated. As shown in recent theoretical work[9], the POZ rearranges to form an electrostatically held dipole complex, which subsequently forms the SOZ. In the gas phase many competing processes are possible, such as dissociation or rearrangement of the COX, followed by bimolecular reactions of the fragment with the CC (or with residual COX) leading to a fairly complex

Fig. 1 →

sequence of events. The unimolecular decomposition of the vibrationally excited COX is currently considered to take place via several distinct routes, like the ester, O-atom, hydroperoxide[10] and other[11] channels the relevance of those was ascribed to the occurrence of the unique indicator products and is dependent on the COX structure and ozonation conditions[10,11]. The hydroperoxide channel (the COX rearrangement into hydroperoxyalkene) is preferred over the ester channel (the COX rearrangement into dioxirane) with COXs possessing a CHR or CH_2R groups in the syn position[12] and it is followed by the O-O bond cleavage to yield OH radical, the species detected in ozonation of alkenes at both low[13] and atmospheric[2d] pressure.

These radicals are thought to play a pivotal role as reactive intermediates in ensuing processes. The lack of solvent stabilization of a highly energy-rich POZ and COX, as well as the absence of the solvent effect (holding CC and CI in close proximity) is believed to result in suppressing the formation of secondary ozonide (SOZ) via association of the CC and the COX, and in enhancing various decomposition/isomerization modes of the COX and other subsequent reactions (Scheme I).

Scheme 1→

Although the parent dioxirane CH_2OO[14] and POZ of ethene[15] have been identified by microwave spectroscopy in the gas phase after the warm-up of the cooled products of ethene ozonation carried out in the solid phase at -196 °C, none of the COX, dioxirane (the product of the ring closure of the COX) and the POZ have ever been detected as intermediate products of the alkene ozonation conducted truly in the gas phase[7,16].

The occurrence of the SOZ in the gas phase ozonation of alkenes has been indicated but not unequivocally proved in earlier studies of the ozonation of several linear and branched-chain alkenes $R_nH_{2-n}C{=}CH_{2-n}R_n$

(n =1,2; R=CH_3 and C_2H_5) *at low pressure* (4-8 Torr)[17]. Photoionization mass spectrometry revealed stable products which are characteristic of a CI decomposition, of reactions of alkenes with OH, and of other free radical reactions. With propene, 2-methylpropene, *cis*-2-butene and *trans*-2-pentene, but not with ethene, trans-2-butene and 2,3-dimethyl-2-butene a very minor peak at m/e (alkene +48) has been detected and tentatively assigned[17] to the SOZ. This assignment was believed to be supported by the observation of the increase of the signal at m/e 104 upon addition of CH_3CHO to *cis*-2-butene + O_3 mixture, which was deemed[17] to reflect a "titration" of the COX ($CH_3(H)COO$) with CH_3CHO (eq. 1).

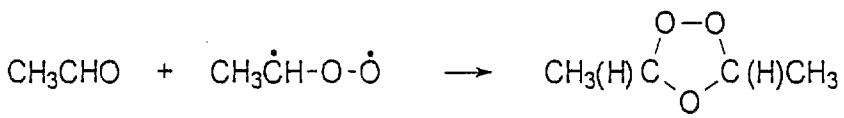

(1)

However, such interpretation[17] will have to be reconsidered in a view of the isomeric products which have been recently proved to originate from the secondary butene-2-ozonide (SBO) rearrangement (eq.2) [18].

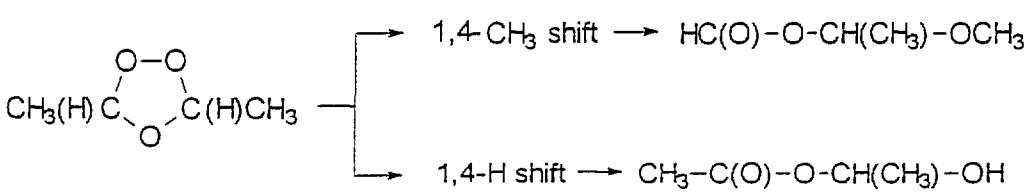

(2)

At *atmospheric pressure*, the SOZs were claimed to appear as minor products of the ozonation of 2-butene[3c] based on the characteristic IR spectrum obtained by subtracting the IR spectral contributions of the other gaseous products, and also of the ozonation of 1-pentene, 1-hexene and 3-

13

heptene (but not of lower homologues) based on the observation of a strong IR absorption band near 9 μm[1c]. Linear reactor-infrared Ar-matrix and microwave spectroscopy examination of the ozonation of *cis*-2-butene[19] and ethene[20] revealed the presence of absorption bands assignable to the SOZ present in a complex mixture of many products for the former but not for the latter reaction. This detection, suffering from concomitant occurrence of other products like esters, epoxides, hydroxyketones and oligomers containing C-O-C and C-O-O-C linkages was, however, not confirmed in a similar matrix isolation FTIR spectral study of the ozonation of *trans*-2-butene in argon containing oxygen[21]. In this examination[21], apart from other compounds, an unknown product was revealed and assigned as 1-hydroxyethyl formate. Its formation was explained by eq. 3.

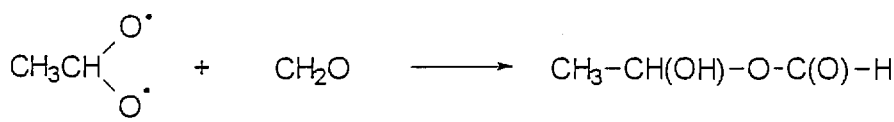

(3)

However, this type of association product, although observed in the gas phase ozonation of ethene[8,22], was not found in the long path FTIR spectral study of the ozonation of *cis*-2-butene in air in the presence of formaldehyde when secondary propene ozonide was observed instead[23]. This observation was explained by eq. 4.

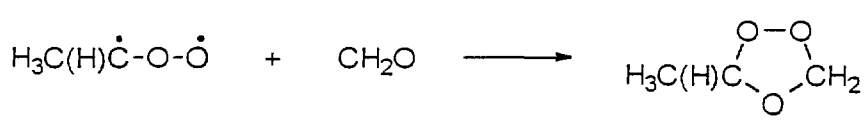

(4)

It was later admitted[24] that the most probable structure of the unknown product is hydroperoxymethyl formate HOO-CH_2-O-CHO which can be formed by association of the two COXs (CH_2COO), or by reaction of the COX

(CH_2COO) with formic acid. This view was recently confirmed by comparing the IR spectrum of the unknown product to that of the synthesized hydroperoxymethyl formate[3e].

Recently, secondary ozonides were observed in the low concentration ozonation of some olefins by deliberately adding carbonyl compounds. Examples are ozonation of ethene in the excess of CH_3CHO or $CH_3C(O)CH_3$ yielding[3d] seconday propene and isobutene ozonide, respectively, and ozonation of 2-butene in the excess of CH_3CHO or HCHO affording[3f], in the given order, secondary butene ozonide and secondary propene ozonide. These experiments confirm that the COX can react with the CCs, but they do not conclusively demonstrate the formation of SOZs from the geminate reaction between the COX and CC.

We have recently shown that the SBO can rearrange to the appropriate esters (eq. 2), and are therefore interested in possible reaction pathways leading to them. Previous work was mainly conducted at room temperature, at which some SOZs are fairly reactive. We have therefore set up a system allowing the measurement of gas phase reactions of some alkenes in the -40 - +20 °C range (and for ethene in the -120 - 0 °C range), which is of atmospheric interest. In contrast with previous investigations, the ozonation products were separated by gas chromatography and identified by both infrared and mass spectroscopy.

In this paper, our previous work on the formation of the secondary butene ozonide (SBO) in the gas phase is extended to include several primary and secondary alkenes. These experiments unequivocally prove that secondary ozonides are formed by ozonation of many alkenes in the gas phase using GC/MS and GC/FTIR techniques.

Our findings provide the first evidence that the bimolecular coupling of the COX and the geminate CC can compete with the COX decompositions in the gas phase, and that the complete Criegee mechanism[7,26] can be extended to the gas phase.

Experimental

The ozonation set-up and analyses of ozonation products

The ozonation of the RHC=CHR (R= CH_3, C_2H_5 and $(CH_3)_2HC$), $RHC=CH_2$ (R= H, C_2H_5, and n-C_4H_9) and $(CH_3)_2C=C(CH_3)_2$ alkenes was carried out by mixing ozone and the alkene (both in excess of nitrogen). For that purpose, 45 Pa of alkene in 50 kPa of N_2, and 135 Pa of ozone in 150 kPa of N_2 were prepared in 2l Pyrex round-bottom flasks which were equipped with P.T.F.E. stopcocks and interconnected via a standard vacuum manifold. Both flasks were preconditioned by keeping them for 30 min either at room temperature, or at 0 - -40 °C when being immersed in a box of 15 l volume containing dry ice - ethanol bath. Thereafter, the ozonation was started by opening the valve interconnnecting both flasks and introducing the O_3-N_2 mixture into the flask containing alkene-N_2. The flask wherein the ozonation took place was immersed in the bath or kept at ambient tempearture for further 30 min. The progress of the ozonation within these 30 min interval was checked by FTIR (a Nicolet, model Impact 400) spectrometry.

The ozonation mixture was then analysed by gas chromatography (a gas chromatograph Shimadzu 14A equipped with FID detector and coupled with a Chromatopac CR5A data processor), GC/MS (a Shimadzu, model QP 1000 quadrupole spectrometer, ionizing voltage 70 eV) and GC/FTIR (a Nicolet,

model Impact 400 coupled to a laboratory-made chromatograph and a chromatograph interphase) techniques. The samples for the GC analysis were withdrawn by a gas-tight syringe directly from the ozonation flask via septum. The GC/MS and GC/FTIR analyses were carried out on total amounts of the ozonation products concentrated in a 4 ml tube which was attached to the vacuum manifold and furnished with a septum and P.T.F.E. stopcock and which was cooled with liquid nitrogen.

Quantitative analyses were performed on a 3.3 m long column packed with SE-30 elastomer on Chromosorb W. A column packed with 2,2'-oxydipropionitrile (3.3 m, 5% on Chromosorb G-HP) was used for the separation of the cis- and trans isomers of SOZs. Other analyses were performed on a 50m long SPIRA KI-5 capillary column. The chromatographic separation of ozonation products was conducted at programmed column temperature. The FID response factors of ozonation products were determined (CH_3CHO 0.30, $(CH_3)\overline{CH\text{-}O\text{-}O\text{-}CH(CH_3)\text{-}O}$ 0.12, CH_3CO_2H 0.24, CH_3CH_2CHO 0.49, CH_2O 0.05, $(C_2H_5)\overline{CH\text{-}O\text{-}O\text{-}CH_2\text{-}O}$ 0.11, $(C_2H_5)\overline{CH\text{-}O\text{-}O\text{-}CH(C_2H_5)\text{-}O}$ 0.14, $CH_3(CH_2)_3CHO$ 0.64, $HC(O)OC_4H_9$ 0.49, $(C_2H_5)\overline{HC\text{-}CH(C_2H_5)\text{-}O}$ 0.72, $(CH_3)_2CHCHO$ 0.66 and $(CH_3)_2HC(H)\overline{C\text{-}O\text{-}O\text{-}C(H)CH(CH_3)_2\text{-}O}$ 0.15) or taken from ref.[27].

Reactants and model compounds

Ozone was prepared in a 250 ml glass reactor furnished with P.T.F.E. stopcock by applying a high-voltage discharge to 3.5 kPa of oxygen (Technoplyn, purity 99%). The yield of ozone was determined by FTIR spectra using the diagnostic absorption band at 1053 cm^{-1}.

trans-2-Butene, 1-hexene, (both Fluka), 1-butene, *trans*-3-hexene, 1-octene (all Aldrich), ethene and 2,3-dimethyl-2-butene (laboratory stock) were of purity higher than 96 % and were distilled on a vacuum line prior to use.

Synthesis of 2,5-dimethyl-3-hexene[28] was accomplished by the reaction of iso-butyl bromide with triphenyl phospine and subsequent treatment the reaction product with n-butyl lithium and iso-butyraldehyde.

Compounds which were used as standards for analysis of FTIR spectra of ozonation mixtures were from the laboratory stock (CO, CH_3CHO, CH_3COOH, CH_3CH_2CHO, CH_3CH_2COOH, CH_4, n-C_4H_{10}, C_2H_6, CH_3OH) or freshly prepared by standard techniques (H_2CO, HCOOH). Their purity was checked by gas chromatography and FTIR spectroscopy.

Preparation of model SOZs

To be able to identify SOZs as produced in the gas phase ozonation of alkenes at -40 - +20 °C, we prepared SOZs in advance at much lower temperatures in the liquid phase and measured their mass and FTIR spectra by applying GC/MS and GC/FTIR spectroscopy techniques to the ozonation mixtures.

All secondary alkene ozonides, except for those of ethene, 1-octene and 2,3-dimethyl-2-butene, were prepared by ozonation of alkenes in a 250 ml tube furnished with P.T.F.E. stopcock and connected to the vacuum manifold. 1-2 kPa amounts of alkene and then of ozone were repeatedly admitted into the tube which was immersed into the ethanol-liquid nitrogen bath and kept at -120°C. Under these conditions the reaction takes place in either the solid or the liquid phase, depending on the alkene. Addition of fresh reactants was performed after the pressure of the previously added ozone decreased to less than 5 % of its original value, indicating its complete reaction. The tube

was left in the cooling bath overnight during which period temperature increased to -20 °C. During that period, the hazardous POZ slowly reacted into mostly SOZ and only small amounts of decomposition products could be detected. The unreacted alkene was removed by pumping the sample at -20 °C.

The secondary octene ozonide (SOO) was obtained by repeatedly admitting 1-octene and ozone into a 300 ml tube kept at -120 °C. The products of the ozonation were concentrated in a 4 ml condenser cooled by liquid nitrogen. After removing the liquid nitrogen bath, the products were slowly warmed up to room temperature and analysed. GC/MS and GC/FTIR analyses on SE 30 column of the gaseous phase did not show any presence of SOO but only heptanal and formaldehyde (major products), so ca. 0.2 ml of diethyl ether was added to the droplets observed on the bottom of the 4 ml tube and the resulting solution was analysed by FTIR, GC/FTIR and GC/MS spectroscopy. The FTIR spectra of the ozonation products after evaporation of ether shown characteristic absorption bands of ozonide (Table 1) and no ν(C=O) absorption band, which indicated that SOO is a major ozonation product. However, GC/FTIR analysis of the ether solution of the droplets revealed three major peaks (Fig. 2). The first two are due to 1-octene and heptanal. The third was found to represent a mixture of heptanal and formic acid, indicating that SOO does not survive at the higher temperatures of the GC analysis (25-80 °C) and decomposes into these two compounds. GC/MS analysis of the etheral solution injected into an empty glass column initially cooled by liquid nitrogen and later slowly warmed up to room temperature shown a big peak of diethyl ether and a smaller peak whose mass fragmentation can be assigned to SOO (Table 1).

Fig. 2→

Table 1→

The secondary ethene ozonide was prepared by admitting 10 kPa of ethene-N_2 (1:1) mixture, and then an O_3 (5 kPa) -N_2 (120 kPa) mixture into a 300 ml tube kept at -120 °C. The reaction mixture was left overnight in the tube whose temperature rose to -50 °C over that period.

The preparation of the secondary tetramethylethene (2,3 dimethyl-2-butene) ozonide was attempted by repeatedly admitting the olefin and ozone into the 300 ml tube kept at - 120 °C, or by carrying out the reaction in pentane at the same temperature. Both attempts failed; the reactions afforded mostly acetone and a mixture of ca. 20 minor products (tetramethyloxirane, tentatively diperoxyacetone and others).

Characterization of model SOZs

All the raw SOZs were analysed by GC/FTIR and GC/MS providing IR and MS spectral data of their pure forms. The data agreed well with published previous work, when available. However, since many of the obtained SOZs were not earlier characterized, we compile both IR and MS spectral data for all the SOZs prepared in this work in Table 1.

Results and Discussion

The formation of SOZs in the gas-phase ozonation of ethene (i), $RHC{=}CH_2$ (R= C_2H_5, and n-C_4H_9) (ii), RHC=CHR (R= CH_3, C_2H_5 and $(CH_3)_2HC$) (iii), and $(CH_3)_2C{=}C(CH_3)_2$ (iv) will be dealt with separately due to some differences (yield, GC response factor of SOZ) observed in each case.

(i) Formation of SOZ in the ozonation of ethene

The gas phase ozonation of ethene at temperatures -120, -50, -20 and 0 °C results in the formation of four observable products, namely formaldehyde,

formic acid, carbon dioxide and secondary ethene ozonide (SEO). Fig. 3 gives the FTIR spectrum of the gaseous ozonation mixture obtained at -120 °C and the spectrum of SEO obtained by removing the contributions of ethene, formaldehyde, carbon dioxide and formic acid. The derived spectrum shows a typical absorption pattern of SEO (see Experimental and ref. 29). The presence of SEO is confirmed by GC/MS analyses of the ozonation mixtures which reveal a minor peak with fragmentation [m/z (rel. intensity, %):76 (3), 46 (28), 45 (22), 44 (34), 30 (36), 29 (100), 28 (28)] assignable (see Experimental and ref. 30) to SEO and which show (Fig. 4) that the yield of SEO diminishes with the increasing ozonation. A quantitative estimate of the ozonation products yields by gas chromatography was not possible, since no SEO peak was observed due to a very low FID response factor. However, both GC/MS and FTIR analysis provide unambiguous evidence that SEO is formed in the gas-phase ozonation of ethene.

We remark that in the previous studies of the reaction between ozone and ethene at low pressure[17,31] or in ppm range in O_2-N_2 mixtures at atmospheric pressure[11,20,22a,24,32] all conducted at room temperature only formaldehyde, formic acid, formic anhydride, CO, CO_2 and a transitory HOO-CH_2-O-CHO[24] (or erroneously assigned HOCH_2-O-CHO [11,22a,b,32]) compound, but no SEO has been detected. The previously observed H_2CO, HCOOH, $(HCO)_2O$, CO and CO_2 compounds, and also H_2CO, HCOOH and CO_2 observed under our low-temperature conditions are indicative of unimolecular decomposition of the energy-rich COX (H_2COO). The previous observation of peroxymethyl formate HOO-CH_2-O-CHO but not of SEO at room temperature might indicate that (i) association of H_2COO with HCOOH is preferred over that of H_2COO with H_2CO, or that (ii) survival of hydroperoxymethyl formate needs less

efficient collisional stabilization than that of SEO. Our results do not allow to discern between these alternatives. However, the most efficient formation of the SEO at -120 °C, the decrease in SEO yield with temperature increasing to -20 °C and no formation of SEO at 0 °C (Fig. 4) indicates that stabilization of hot SEO or the CI is indeed an important factor.

The above temperature dependence of the SEO yield thus reveals that the observation of bimolecular reaction between H_2COO and H_2CO to SEO is enabled by cooling the gaseous reaction mixtures to low temperatures which helps in preventing fragmentation of the reactants and/or of the nascent SEO. The earlier proposed[11,22a,b,32] transient formation of hydroxymethyl formate has been now abandoned[3,24], since this compound has not been yet observed. Nevertheless, we wish to note that hydroxymethyl formate formation can occur via the previously assumed[11,22a,b,32]reaction between the COX and H_2CO, or via 'hot' SEO decomposition involving the split of the ring O-O bond and 1,4 H-shift (eq. 5),

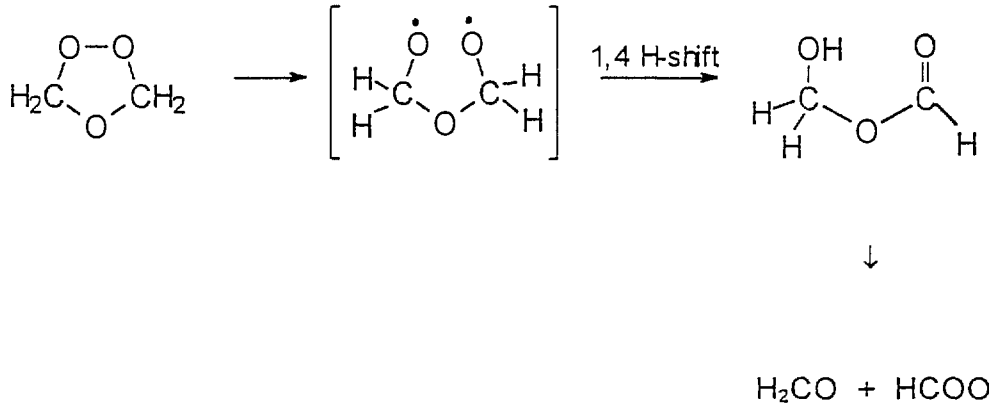

(5)

the route observed in the laser-induced thermal decomposition of secondary butene ozonide[18]. We further note that the thermal gas-phase decomposition of SEO affords[33] equimolar amounts of HCOOH and H_2CO, and even though it was postulated to occur via $HOCH_2$-O-CHO, this transient has never been directly detected. Also our FTIR spectral examination of SEO decomposition at 150 °C confirmed HCOOH and H_2CO as two major products and did not reveal any $HOCH_2$-O-CHO. We believe, however, that $HOCH_2$-O-CHO must be precursor of the final HCOOH and H_2CO products and would like to confirm it by attempting its detection in laser-photosensitized (and heterogeneous contributions obviating) decomposition of SEO which is under way.

(ii) Formation of SOZ in ozonation of $RHC{=}CH_2$

The gas-phase ozonation of $RHC{=}CH_2$ (R= C_2H_5, and n-C_4H_9) at -40, -20, 0 and 20 °C yields a number of products among those secondary ozonides are important ones.

Thus the ozonation of 1-butene yields CO, CO_2, H_2CO, secondary butene ozonide (SB1O) and propionic acid, and that of 1-hexene gives CO, CO_2, H_2CO, valeraldehyde, n-butyl formate, butyloxirane and secondary hexene ozonide (SH1O) (Fig. 5). The ozonides separated by gas chromatography were characterized by their mass fragmentation [m/z (rel. intensity, %) for SB1O 104 (1, $M^{\cdot+}$), 75 (10), 58 (9), 57 (12), 47 (8), 46 (6), 45 (10), 42 (11), 41 (7), 31 (23), 30 (17), 29 (100), 38 (35), 27 (37); for SH1O 104 (1, M-28), 90 (4), 75 (7), 73 (6), 71 (5), 60 (17), 58 (16), 57 (23), 55 (9), 45 (14), 44 (59), 43 (25), 42 (15), 41 (57), 39 (22), 31 (12), 30 (11), 29 (100), 28 (26), 27 (42). While a very small signal for the molecular ion is observed for SB1O,

Fig. 5 →

the highest m/z signal for SH1O corresponds to a M-28 fragment. FTIR spectra of both chromatographically separated ozonides are given in Fig 6; they are characteristic of secondary ozonides[22c,23,29] and contain no carbonyl absorption bands. We stress that both the FTIR and MS data of the ozonides chromatographically separated from the gaseous ozonation mixtures match those of the secondary ozonides prepared as standards (see Experimental).

Fig. 6 →

While there are several distinctive routes for the formation of the observed products and while CO and CO_2 are regarded as formed by multistep reactions[8,10,11], the aldehydes and carboxylic acids can be rationalised as formed, apart from other routes[8,10,11], by the direct SOZ decomposition [18,33]. Both secondary ozonides are stable in the gaseous mixtures and do not decompose at room temperature within several hours. The yields of SB1O and SH1O steeply decrease with the increasing ozonation temperature and are at the each temperature very similar (Fig. 6). The almost identical slopes of their yield vs. temperature plots indicate that the formation of the SOZ from the primary alkenes $RHC{=}CH_2$ is not affected by the length of the R group. The significantly lower yields of both $RHC{=}CH_2$ SOZs at higher temperatures may explain why the two SOZs can escape detection in studies conducted at ambient temperatures. This steep yield vs. temperature plot seen with the primary but not secondary alkene SOZs (Fig. 6) can be explained by lower stability of H_2COO compared to RHCOO, this difference being more pronounced as temperature increases. This view is corroborated in Table 2 which shows that while the yield of the rearranged products of H_2COO (HCOOH) and of RHCOO (RCOOH) with higher temperature slightly decrease, the yield of RH (decomposition product of RHCOO) slightly

increase, and the yield of CO and CO_2 (decomposition products of H_2COO) increase more profoundly.

Table 2→

The gas-phase ozonation of 1-octene ($RHC{=}CH_2$, R= n-C_6H_{13}) was carried out, due to low volatility of this alkene at low temperatures, only at 20 °C and the obtained ozonation mixture was concentrated in the 4 ml tube cooled with liquid nitrogen and subsequently warmed up to room temperature. Both gas and liquid phase (droplets) were produced and analysed. GC/MS and GC/FTIR analyses on the SE 30 column of the gaseous phase revealed the presence of heptanal, formaldehyde, hexane, hexyloxirane and hexyl formate, but no secondary octene ozonide (SOO).

We note that hexyloxirane was observed[34] as a product of the ozonation of octene at atmospheric pressure together with isomeric octanal and 2-octanone and that our GC/FTIR technique shows that of these three products only hexyloxirane is formed under our experimental conditions. GC/FTIR analysis of the gas phase and that of etheral solution of the liquid phase are very different and are compared in Fig. 7. While the former indicates the presence of 1-octene, heptanal, hexyloxirane and hexyl formate, the latter reveals 1-octene, heptanal and a broad peak the IR spectrum of which is composed of contributions of hexyl formate, heptanal, formic acid and hexyloxirane. Considering that retention times of formic acid and heptanal differ from that of the broad peak, we can assume that these two compounds are products of the SOO decomposition. This decomposition is supported by the data in the Experimental Section (Fig. 1). We assume that the SOO → HCOOH + $C_6H_{13}CHO$ decomposition is facilitated at higher temperatures, since the FTIR spectrum of the crude liquified ozonation product (the etheral solution of the droplets from which ether evaporated) exposed only to room

Fig. 7→

temperature is fully compatible with the FTIR spectrum of SOO. This is proved in Fig. 8 showing the same FTIR spectral pattern of SB1O and SH1O and of the crude product. We can thus conclude that SOO escapes direct gas-phase observation due to its low volatility and stability, but it is an important product in the gas phase ozonation of 1-octene.

Fig. 8→

Up to now, studies of reaction products in the gas-phase ozonation of primary alkenes were restricted only to the the ozonation of propene[11,17] and 1-octene[34] which revealed a number of products but no SOZ. Our results on the gas phase ozonation of the $RHC{=}CH_2$ (R= C_2H_5, n-C_4H_9 and n-C_6H_{13}) prove that secondary ozonides of these alkenes are produced in substantial amounts and that they are in the gas phase at room temperature.

(iii) Formation of SOZs in the ozonation of RHC=CHR

The gas phase ozonation of RHC=CHR (R=CH_3, C_2H_5 and $(CH_3)_2CH$) carried out at -40, -20, 0 and 20 °C yields, apart from other products, secondary ozonides in relatively high yields. Typical GC traces of the ozonation mixtures obtained by reacting ozone and alkene at the lowest temperature are shown in Fig. 9. It is found that the products of the ozonation of *trans*-2-butene are CO, CO_2, CH_4, CH_3CHO, CH_3OH and *cis*- and *trans*-secondary butene ozonides (SBO), the products of the ozonation of *trans*-3-hexene are CO, CO_2, C_2H_6, CH_3CH_2CHO, diethyloxirane and *cis*- and *trans*-secondary hexene ozonides (SHO), and the products of the ozonation of *trans*-2,2-dimethyl-3-hexene are CO, CO_2, $(CH_3)_2CHCHO$, $C_{16}H_{24}$ and *cis*- and *trans*-secondary 2,2-dimethylhexene ozonides (SDO). As in the previous instances (see (ii)), CO and CO_2 can be regarded as products of several

Fig. 9→

reaction sequences, and RCHO (along with unobserved RCOOH) can arise, apart from other routes[8,10,11], from decomposition of SOZ[18,33].

The secondary ozonides were identified using the GC/FTIR procedure through their FTIR spectra (Fig. 10) and characterised by mass fragmentation [m/z (rel. intensity, %):

for SBO - 104 (5), 89 (16), 72 (5), 61 (8), 60 (11), 45 (40), 44 (34), 43 (100), 31 (10), 29 (34), 28 (8);

for SHO - 132 (2), 103 (18), 59 (17), 58 (31), 57 (43), 47 (9), 42 (10), 41 (11), 31 (24), 30 (12), 29 (100), 28 (33), 27 (26);

for SDO - 117 (M-$(CH_3)_2CH$, 1), 84 (2), 73 (7), 72 (8), 56 (8), 54 (6), 43 (100), 41 (27), 29 (10), 28 (6), 27 (17) and other minor signals.

Fig. 10 →

The mass spectra of the SOZ show that the molecular ion is observed only with SBO (m/z 104) and SHO (m/z 132), while for the SDO the highest m/z fragment corresponds to M-R.

The total yields of the SOZs (combined yield of the *cis*- and *trans*-isomers) from the symmetric secondary RHC=CHR alkenes differ considerably depending on the R group size and are much less temperature dependent than in the case of the primary $RCH=CH_2$ alkenes (Fig. 6). The SOZ yields for R = CH_3, C_2H_5 and $(CH_3)_2HC$ noticeably increase in the given order at each temperature and reveal the stabilising effect of bulkier substituent. The very small temperature dependence of the yields of SOZs from the RHC=CHR, together with a fairly significant temperature dependence of the yields of SOZ from the $RHC=CH_2$ is in line with the assumed different stability of the involved COXs at different temperatures. In other words, the reason for the increased yield at low temperatures of SB1O and SH1O is more efficient

21

stabilization of the H_2COO intermediate, a species not involved in the ozonation of RHC=CHR.

Previous studies on the gas-phase ozonation of RHC=CHR alkenes which were aimed at the identification of ozonation products dealt with cis-2-butene [2a,13a,17,19,23], trans-2-butene[2a, 10a,11,21,35] and trans-2-pentene[17]. In these studies SOZs have been suggested but not unambiguously identified. Similarly to the reaction in solution [7d,36], the ozonation of *trans*-RHC=CHR alkenes in the gas phase is stereospecific. The ratios of the *trans*- and *cis*- SOZ isomers (given in Table 3) reveal the preference of the *trans*-SOZ forms, which is also true for the solution ozonation where the cis/trans ozonide ratio depends on the solvent, the presence of complexing agents, and the warm-up rate of the ozonation reaction mixture[7d,36]. The deviations from stereo randomization in the solvent-phase ozonation of *trans*-RCH=CHR alkenes carried out in non-polar hydrocarbons is greater for R=$(CH_3)_3C$ (*trans/cis* ratio 2.6 and higher) and smaller with less bulky R (*trans/cis* ratio ca. 1.2-1.5 for $(CH_3)_2HC$, CH_3CH_2 and CH_3 groups)[7d]. Our data show that the preference for the *trans* isomer in the gas phase is comparable to that observed in solution with R = $(CH_3)_2HC$ and CH_3CH_2 and somewhat higher with R = CH_3.

Table 3 →

The observed ratios of SOZs can be qualitatively explained in terms of the original Criegee mechanism[26] and of its recent refinement[9a] by adopting the view that the COX and CC formed upon the dissociation of the POZ are not separated but form a complex that subsequently transforms to the SOZ. The recent view on the POZ-SOZ transformation[9b] involves two types of rotation of the CC with respect to the COX, the one taking place in the plane of heavy atoms and maintaining the steric structure, and the other taking place in a perpendicular plane and inverting it. The explanation of the higher preference

28

of the trans isomers of SBO and SHO in the absence of solvent can be thus related to an easier 'in plane' rotation, even though the reasons for promoting this type of rotation by absence of solvent are not clear. In any case, this stereospecificity is a strong indication of geminate pair recombination. Reactions between randomly oriented reactants may lead to smaller selectivity, although the AM1 calculations of Ref.9b indicate a smaller barrier for the prefered route, making it possible that selectivity will be observed also for secondary reactions. This point may be tested by adding intentionally excess carbonyl compounds and analyzing the the *cis/trans* ozonide ratio.

(iv) Failed formation of SOZ in the ozonation of 2,3-dimethyl-2-butene

The gas phase ozonation of $(CH_3)_2C{=}C(CH_3)_2$ carried out at -40 °C does not yield secondary tetramethylethene ozonide (STO) but only acetone (major product) and acetone diperoxide together with a C_4H_8O and two other minor products.

These findings are in keeping with other unsuccessful attempts to prepare STO in the gas phase at low[6,37] or atmospheric[38] pressure, in solution[7c], in silica gel[39] and in cryogenic matrices[40]. We note, however, that the successful formation of STO occurs on the surface of polyethene particals when restricted migration of the adsorbed CC and COX is believed[41] to overwhelm low reactivity of the CC in intramolecular cyclization with COX. The absence of STO among the products of the gas-phase ozonation of tetramethylethene is thus confirming the failure of the STO formation in solution phase.

Summary

The ozonation of a series of alkenes in the gas phase is unequivocally shown to produce, apart from the other products, secondary ozonides whose occurrence in this reaction has been up to now only surmised. The yields of the primary alkenes ($RHC=CH_2$) decrease as the temperature is increased from -40 to 20 °C, while those of secondary alkenes (*trans*-RHC=CHR) are almost unaffected within this temperature range. The stereoselectivity for the formation of *trans*-secondary ozonides from *trans*-RHC=CHR possessing Me, Et, and i-Pr is similar to the ozonation in solution. These data show that the complete Criegee mechanism, applied up to now only to the liquid phase, can be extended to the gas-phase, and that the geminate CO and COX components can bimolecularly react into SOZ even without stabilizing effect of solvent.

Our results also indicate that the formation of SOZs in the gas phase should not be ignored, particularly at low temperatures. Reactions of SOZs should therefore be considered in any future model of the atmospheric chemistry of ozone.

Acknowledgment. This research was supported under Grant No. HRN-2078, C12-223, US-Israel Cooperative Development Research Program, Office of the Science Advisor, US Agency for International Development, and under Grant No. 104/96/0472 of thr Grant Agency of the Czech Republic.

References

(1) (a) Hanst, P. L.; Stephens, E. R.; Scott, W. E. *Proc. API* **1955**, 35, 175, (b) Scott, W. E.; Stephens, E. R.; Hanst, P. L.; Doerr, R. C. Proc. API 1957, 37, 171, (c) Hanst, P. L.; Stephens, E. R.; Scott, W. E.; Doerr, R. C. *Prepr. Div. Petrol. Chem., ACS*, **1959**, 4, A-7.

(2) e.g. (a) Altshuller, A. P.; *Atmos. Environ.* **1983**, 17, 2383, (b) Atkinson, R; Carter, W. P. L. *Chem. Rev.* **1984**, 84, 437, (c) Grosjean, D. *Environ. Sci. Technol.* **1990**, 24, 1428, (d) Atkinson, R.; Aschmann, S. M. *Environ. Sci. Technol.* **1993**, 27, 1357, (e) Grosjean, D.; Williams, E. L.; Grosjean, E. *Environ. Sci. Technol.* **1993**, 27, 830,

(3) (a) Atkinson, R.; Tuazon, E. C.; Aschmann, S. M. *Environ. Sci. Technol.* **1995**, 29, 1860. (b) Horie, M.; Neeb, P.; Moortgat, G. K. *Int. J. Chem. Kinet.* **1997**, 29, 461. (c) Horie, M.; Neeb, P., Moortgat, G. K. *Int. J. Chem. Kinet.* **1994**, 26, 1075. (d) Neeb, P.; Horie, O.; Moortgat, K. K. *Tetrahedron Lett.* **1996**, 37, 9297. (e) Thamm, J., Wolff, S.; Turner, W. V.;Gäb, S.; Thomas, W., Zabel, F; Fink, E. H.; Becker, K. H. *Chem. Phys. Lett.* **1996**, 258, 155. (f) Grosjean, E., Grosjean, D. *Int. J. Chem. Kinet.* **1996**, 28, 911. (g) Gutbrod, R.; Kraka, E.; Schindler, R. N.; Cremer, D. *J. Am. Chem. Soc.* **1997**, 119, 7330.

(4) Seinfeld, J. H. *Science* **1989**, 243, 745.

(5) Zimmermann, P. R.; Greenberg, J. P. Westberg, C. E. *J. Geophys. Res.* **1988**, 93D, 1407.

(6) e.g. Gäb, S.; Hellpointner, E.; Turner, W. V.; Korte, F. *Nature* **1985**, 316, 535.

31

(7) (a) Kuczkowski, R. L. *Chem. Soc. Rev.* **1992**, 79. (b) Zvilichowski, G. in *The Chemistry of hydroxyl, ether and peroxide groups*, Vol. 2, Suppl. E, Patai, S. ed., Wiley, New York, 1993, (c) Bailey, P. S. *Ozonation in organic chemistry*, Academic Press, New York, Vol. I, 1978,; Vol. II, 1982. (d) Kuczkowski, R. L. *in 1,3-Dipolar cycloaddition chemistry*, Padwa A., ed.,Wiley, New York, Vol. 2, Ch. 11, 1984.

(8) Herron, J. T.; Martinez, R. I., Huie R. E. *Int. J. Chem. Kinet.* **1982**, 14, 20.

(9) (a) Cremer, D.; Kraka, E.; McKee, M. L.; Radhakrishnan, T. P. *Chem. Phys. Lett.* **1991**, 187, 491. (b) Ponec, R.; Yuzhakov, G.; Haas, Y.; Samuni, R. *J. Org. Chem.* **1997**, 62, 2757.

(10) (a) Martinez, R. I.; Herron, J. T. *J. Phys. Chem.* **1988**, 92, 4644, (b) Martinez, R. I.; Herron, J. T. *J. Phys. Chem.* **1987**, 91, 946.

(11) Horie, O.; Moortgat, G. K. *Atmos. Environ.* **1991**, 25A, 1881.

(12) Gutbrod, R.; Kraka, E.; Schindler, R. N.; Cremer, D. *J. Am. Chem. Soc.* **1997**, 119, 7330.

(13) (a) Finlayson, B. J.; Pitts, J. N.; Atkinson, R. J. *Am. Chem. Soc.* **1974**, 96, 5356, (b) Martinez, R. I.; Huie, R. E.; Herron, J. T. *Chem. Phys. Lett.* **1980**, 72, 443.

(14) (a) Lovas, F. J.; Suenram, R. D.; *Chem. Phys. Lett.* **1977**, 51, 453. (b) Suenram, R. D.; Lovas, F. J. *J. Am. Chem. Soc.* **1978**, 100, 5117, (c) Martinez, R. I.; Huie, R. E.; Herron, J. T. *Chem. Phys. Lett.* **1977**, 51, 457.

(15) Zozom, J.; Gillies, C. W.; Suenram, R. D.; Lovas, F. J. *Chem. Phys. Lett.* **1987**, 139, 64.

(16) (a) Sander, W. *Angew. Chem., Int. Ed. Engl.* **1989**, 29, 344, (b) Bunnelle, W. H. *Chem. Rev.* **1991**, 91, 335.

(17) Martinez, R. I.; Herron, J. T.; Huie, R. E. *J. Am. Chem. Soc.* **1981**, 103, 3807.

(18) Khachatryan, L.; Fajgar, R.; Haas, Y.; Pola, J. *J. Chem. Soc., Perkin Trans. 2* **1996**, 1981.

(19) Kühne, H.;Foster, M.; Hulliger, J.; Ruprecht, H. Bauder, A.; Günthard, H-H. *Helv. Chim. Acta* **1980**, 63, 1971.

(20) Kühne, H.;Vaccani, S.; Bauder, A.; Günthard, H-H. *Chem. Phys.* **1978**, 28, 11.

(21) Horie, O.; Moortgat, G. M. *Chem. Phys. Lett.* **1989**, 156, 39.

(22) (a) Su, F.; Calvert, J. G.; Shaw, J. H. *J. Phys. Chem.* **1980**, 84, 239, (b) Kan, C. S.; Su, F.; Calvert, J. G.; Shaw, J. H. *J. Phys. Chem.* **1981**, 85, 2359, (c) Niki, H.; Maker, P. D.; Savage, C. M.; Breitenbach, L. P. *J. Phys. Chem.* **1981**, 85, 1024.

(23) Niki, H.; Maker, P. D.; Savage, C. M.; Breitenbach, L. P. *Chem. Phys. Lett.* **1977**, 46, 327.

(24) Neeb, P.; Horie, O.; Moortgat, G. K. *Chem. Phys. Lett.* **1995**, 246, 150.

(25) Fajgar, R.; Vítek, J.; Haas, Y.; Pola, J. *Tetrahedron Lett.* **1996**, 19, 3391.

(26) (a) Criegee. R. *Rec. Chem. Prog.* **1957**, 18, 111. (b) Criegee, R. *Angew. Chem.* **1975**, 87, 765.

(27) Dietz, W. A. *J. Gas. Chromatog.* **1967**, 5, 68.

(28) Bohlmann, F.; Mannhardt, H. *Chem. Ber.* **1955**, 88, 1333.

(29) (a) Garvin, D.; Schubert, C. *J. Am. Chem. Soc.* **1956**, 60, 807. (b) Niki, H.; Maker, P. D.; Savage, C. M.; Breitenbach, L. P. *Environ. Sci. Technol.* **1983**, 17, 312A.

(30) (a) Gillies, C. W.; Latimer, R. P.; Kuczkowski, R. L. *J. Am. Chem. Soc.* **1974**, 96, 1536. (b) Castonguay, J.; Bertrand, M.; Carles, J.; Fliszár, S.; Rousseau, Y. *Can. J. Chem.* **1969**, 47, 919. (c) Murray, R. W.; Hagen, R. *J. Org. Chem.* **1971**, 36,1103

(31) Herron, J. T.; Huie, R. E. *J. Am. Chem. Soc.* **1977**, 99, 5430.

(32) Niki, H.; Maker, P. D.; Savage, C. M.; Breitenbach, L. P. *J. Phys. Chem.* **1981**, 85, 1024.

(33) Hull L. A.; Hisatsune, I. C.; Heicklen, J. *J. Phys. Chem.* **1972**, 76, 2659.

(34) Paulson, S. E.; Seinfeld, J. H. *Environ. Sci. Technol.* **1992**, 26, 1165.

(35) Walte, T. A.; Bufalini, J. J.; Gay, B. W. *Environ. Sci. Technol.* **1977**, 11, 382.

(36) (a) Murray, R. W.; Youssefyeh, R. D.; Story, P. R. *J. Am. Chem. Soc.* **1967**, 89 2429. (b) Bailey, P. S.; Ferrell, T. M. *J. Am. Chem. Soc.* **1978**, 100, 899. (c) Bailey, P. S.; Ferrell, T. M.; Rustaiyan, A.; Seyhan, S.; Unruh, L. E. *J. Am. Chem. Soc.* **1978**, 100, 894.

(37) Martinez, R. I.; Herron, J. T. J. Phys. Chem. **1987**, 91, 946.

(38) Niki, H.; Maker, F. D.; Savage, C. M.; Breitenbach, L. P.; Hurley, M. D. *J. Phys. Chem.* **1987**, 91, 941.

(39) Aronovitch, C.; Tal, D.; Mazur, Y. *Tetrahedron Lett.* **1982**, 3623.

(40) Samuni, U.; Haas, Y.; Fajgar, R.; Pola, J. *manuscript in preparation.*

(41) Griesbaum, K. Volpp, W.; Greinert, R. *J. Am. Chem. Soc.* **1985**, 107, 5309.

Captions to Figures

Figure 1.

Computed energy profile for *cis*-2-butene ozonation (according to Ref. 9b).

Figure 2.

GC/FTIR analysis of the mixture in diethyl ether obtained by ozonation of 1-octene at -120 °C.

Figure 3.

FTIR spectrum of the mixture obtained by ozonation of ethene at -120 °C (a) and of SEO attained by subtraction of the contributions of CH_2O and HCO_2H (b).

Figure 4.

Comparison of GC/MS traces of the mixtures obtained by ozonation of ethene at -120 (a), -50 (b), -20 (c) and 0 °C (d). In the traces reflecting the same injected gaseous amounts of the ozonation mixture the first peak represents a blend of N_2, C_2H_4 and CH_2O, and the second relates to SEO.

Figure 5.

Typical GC/MS trace of ozonation mixtures.

(a) 1-butene - O_3 - (SE 30 column, programmed temperature 25-75 °C). Peak identification: 1 - air, CO, CO_2, 1-butene; 2 - CH_2O; 3 - CH_3CH_2CHO - SB1O; 5 - C_8H_{16}; 6 - CH_3CH_2COOH.

(b) 1-hexene - O_3 - (SE 30 column, programed temperature 20-120 °C). Peak identification: 1 - air, CO, CO_2, n-C_4H_{10}, CH_2O; 2 - 1-hexene; 3 - $CH_3(CH_2)_3CHO$; 4 - n-C_4H_9 OC(O)H; 5 - n-butyloxirane; 6 - SHO.

Figure 6.

Yields of secondary ozonides as dependent on the ozonation temperature.

a - 1-butene; b - 1-hexene; c - *trans*-2-butene; d - *trans*-3-hexene; e - *trans*-2,5-dimethyl-3-hexene.

Figure 7.

GC/FTIR trace of gas phase (a) and of etheral solution of liquid phase (b) resulting from ozonation of 1-octene carried out at 20 °C.

Column SE 30, programmed temperature 20-120 °C. Peak identification: 1 - diethyl ether, 2 - 1-octene, 3 - heptanal, 4 - hexyl formate, 5 - hexyloxirane, 6 - heptanal, formic acid, hexyl formate and hexyloxirane, 7 - heptanoic acid.

Figure 8.

Comparison of the FTIR spectrum of the crude product (SOO) from ozonation of 1-octene obtained at -120 °C (a), 20 °C (b), and that of SB1O (c) and SH1O (d).

Figure 9.

GC trace of ozonation products of *trans*-2-butene (a) , *trans*-3-hexene (b) and *trans*-2,5-dimethyl-3-hexene (c) obtained at -40 °C.

(a) (2,2'-oxydipropionitrile column, temperature programmed between 25-50 °C). Peak identification: 1 - air, CO, CO_2, CH_4; 2 - *trans*-2-butene; 3 - CH_3CHO; 4 - CH_3OH; 5 - *trans*-SBO, 6 - *cis*-SBO.

(b) (2,2'-oxydipropionitrile column, temperature programed between 30-70°C). Peak identification: 1 - air, CO, CO_2, C_2H_6, 2 - *trans*-3-hexene; 3 - CH_3CH_2CHO; 4 - diethyloxiran; 5 - *trans*-SHO, 6 - *cis*-SHO.

(c) (2,2'-oxydipropionitrile column, temperature programmed between 30-70 °C). Peak identification: 1 - air, CO, CO_2, 2 - $(CH_3)_2CHCHO$, 3 - *trans*-2,5-dimethyl-3-hexene, 4 - $C_{16}H_{24}$, 5 - *cis*-SDO, 6 - *trans*-SDO.

Figure 10.

FTIR spectra of SBO (a), SHO (b) and SDO (c) as obtained by GC/FTIR spectroscopy.

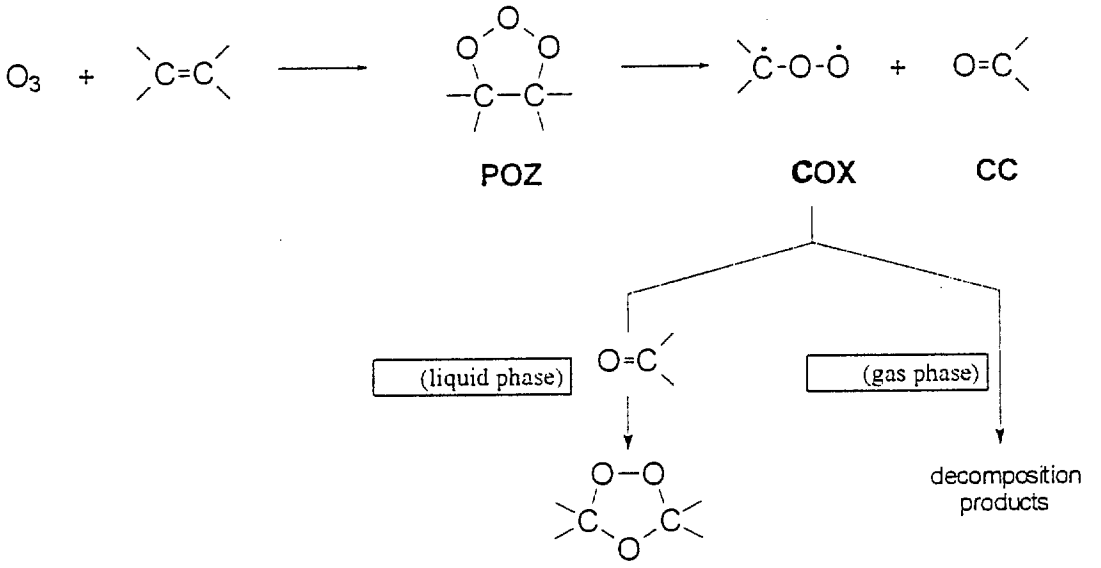
O3
POZ
COX
CC
(liquid phase)
(gas phase)
decomposition products

Scheme I

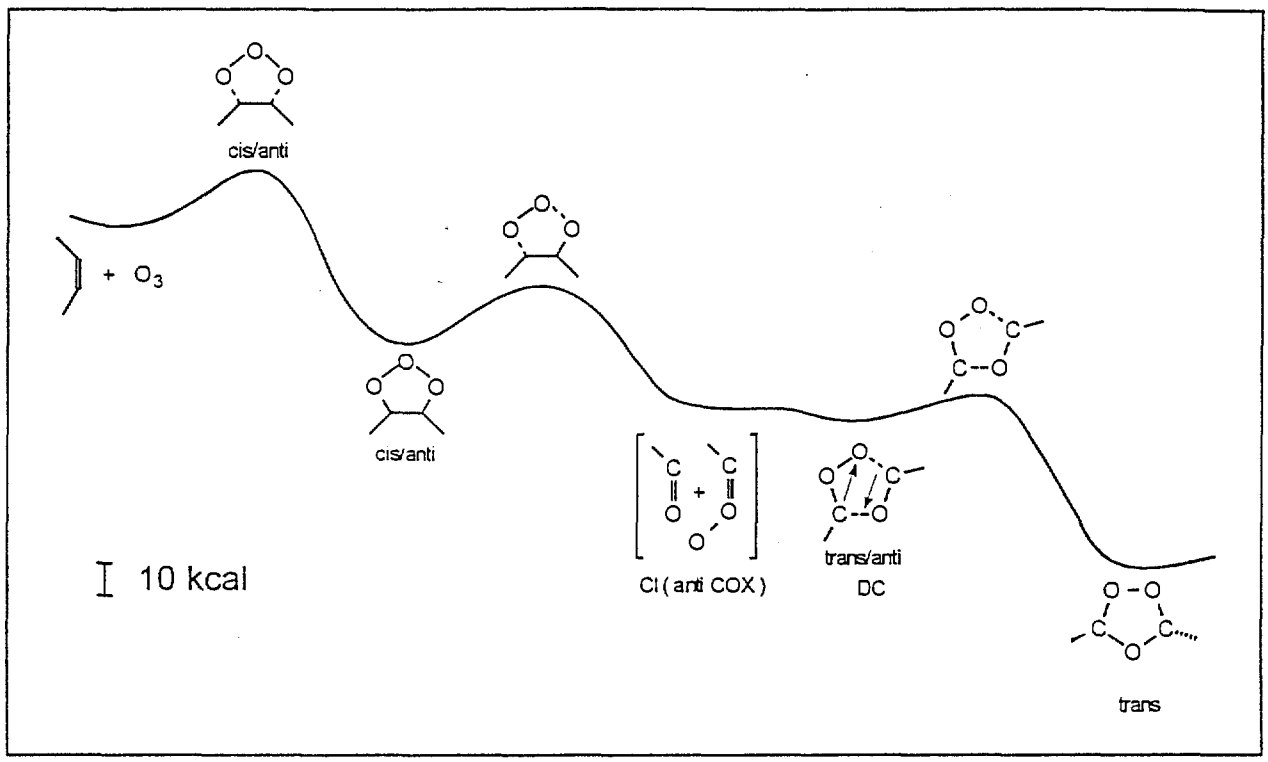

FIG 1

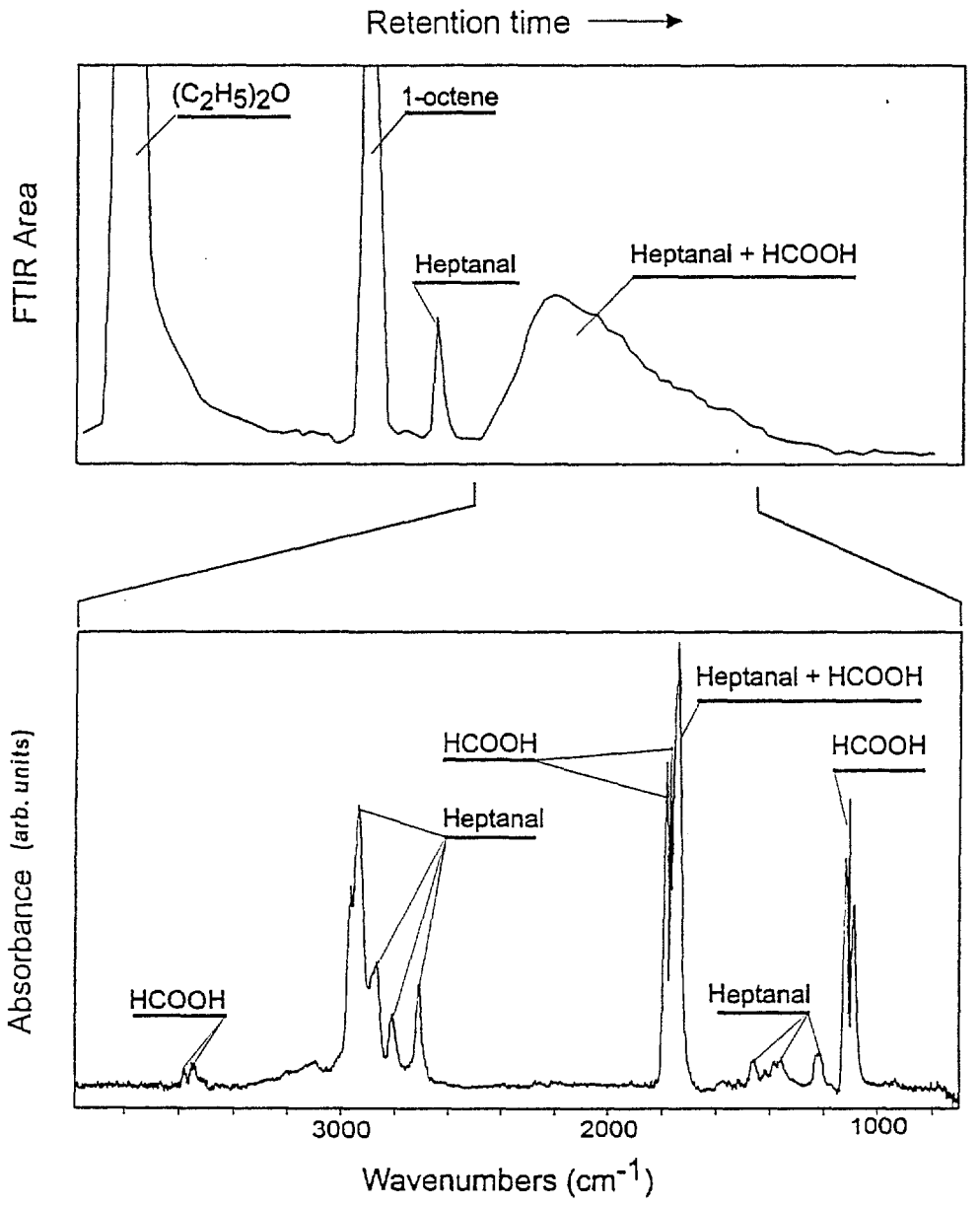
Retention time
FTIR Area
$(C_2H_5)_2O$
1-octene
Heptanal
Heptanal + HCOOH
Absorbance (arb. units)
Heptanal + HCOOH
HCOOH
HCOOH
Heptanal
HCOOH
Heptanal
3000
2000
1000
Wavenumbers (cm^{-1})

FIG 2

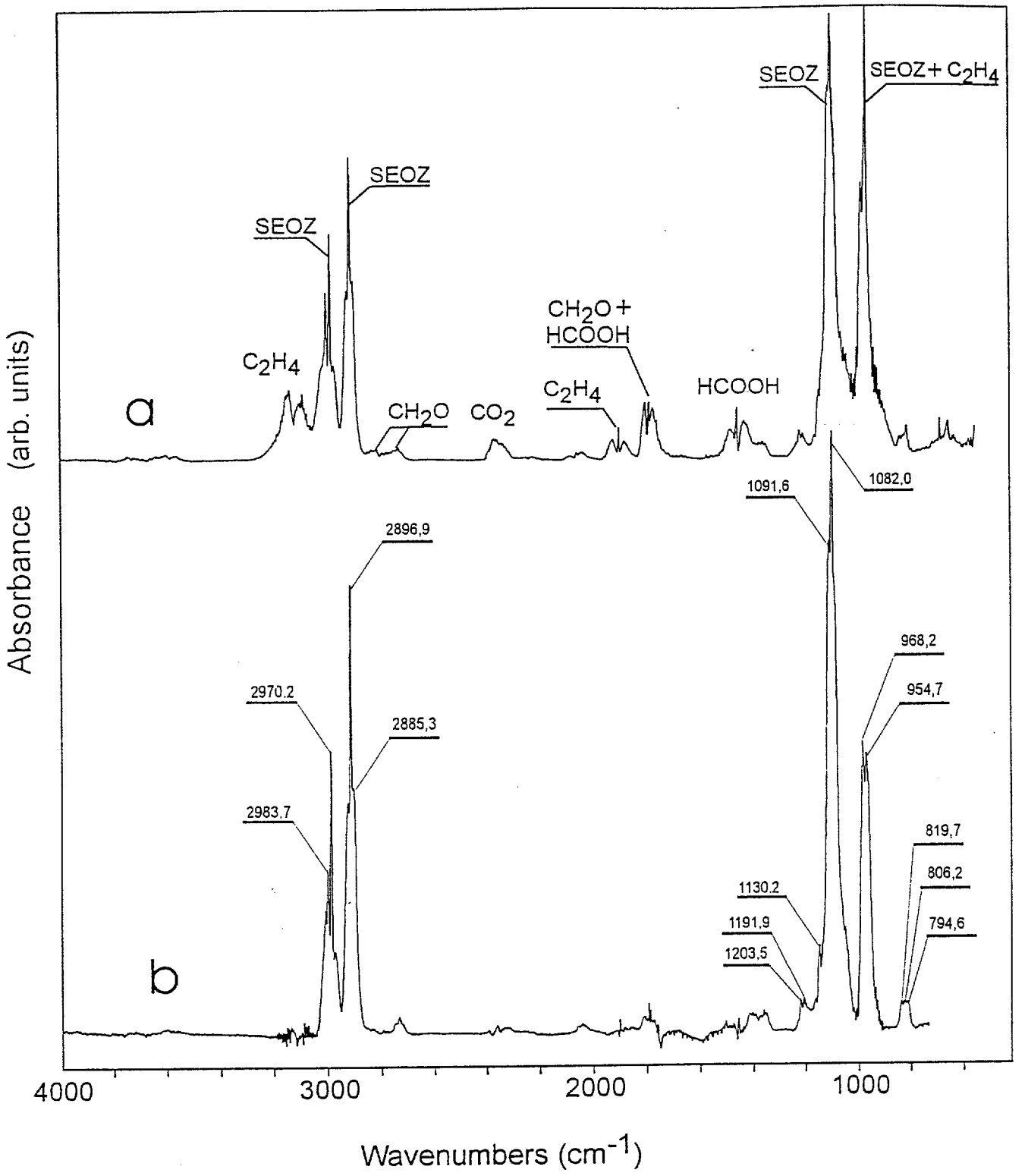
SEOZ
SEOZ+ C_2H_4
SEOZ
SEOZ
CH_2O + HCOOH
C_2H_4
C_2H_4
CH_2O
CO_2
HCOOH
a
1091,6
1082,0
2896,9
968,2
954,7
2970.2
2885,3
2983.7
819,7
806,2
1130.2
1191,9
794,6
1203,5
b
Absorbance (arb. units)
4000
3000
2000
1000
Wavenumbers (cm^{-1})

FIG 3

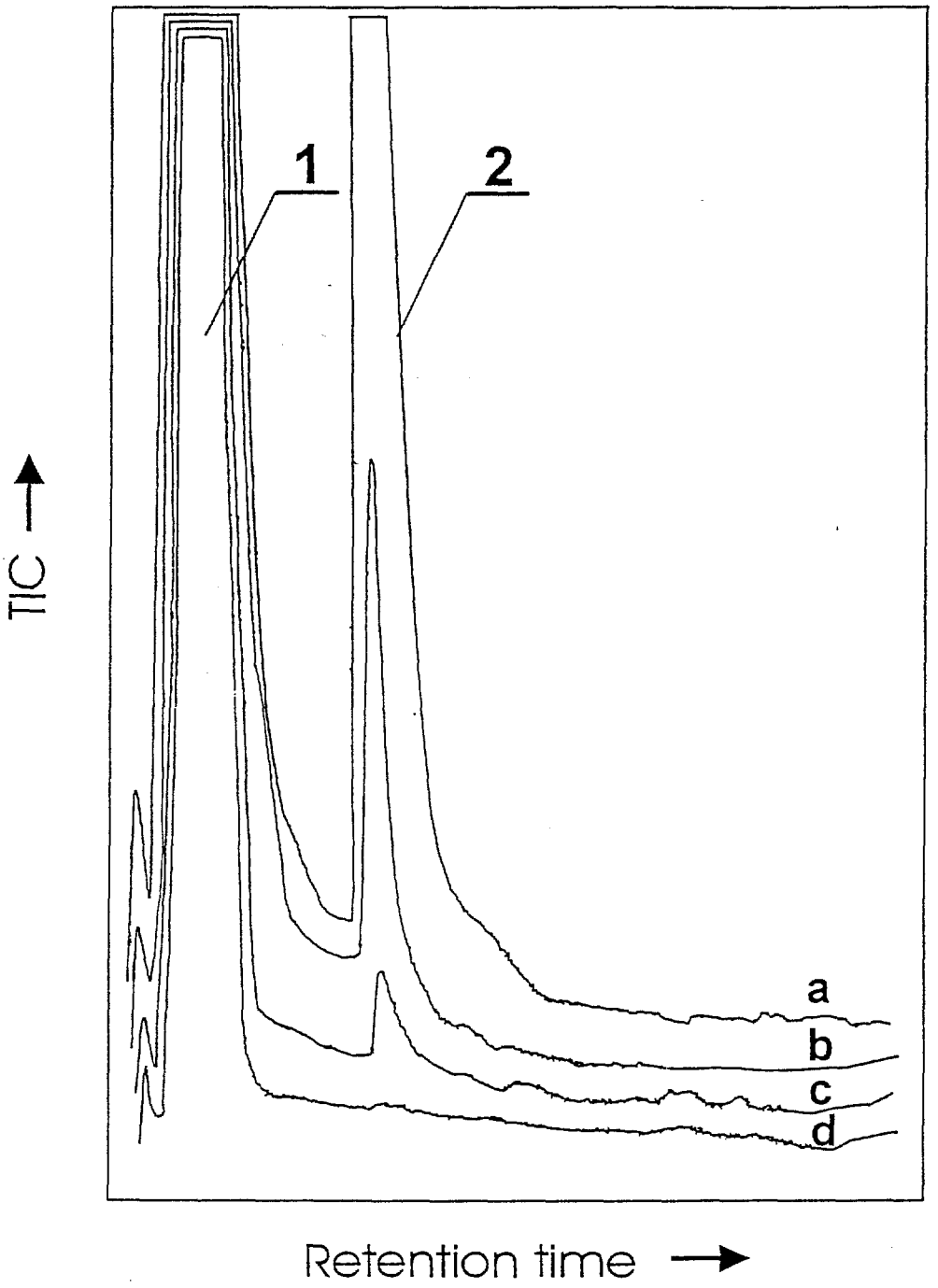

FIG 4

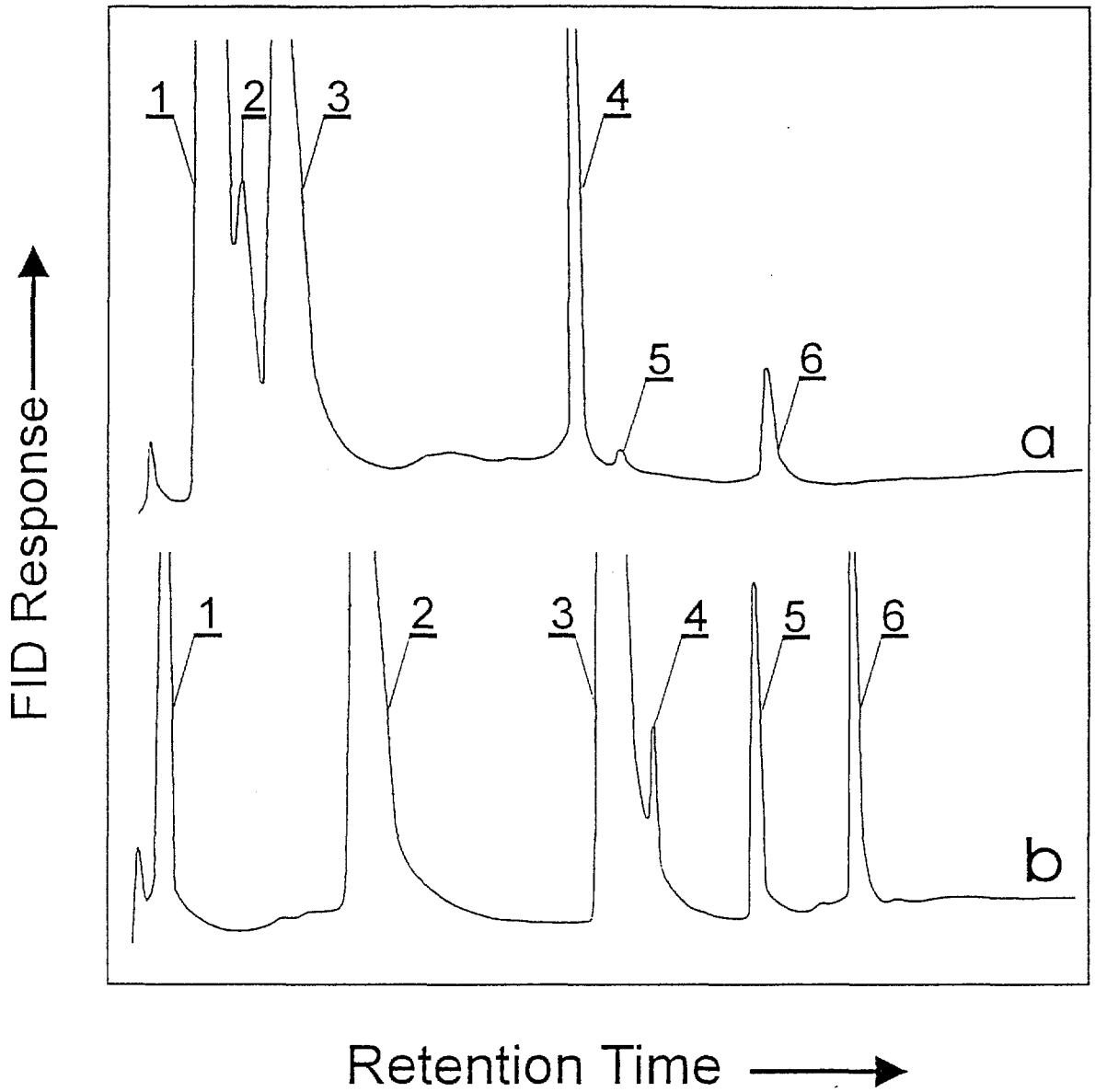

FIG 5

43

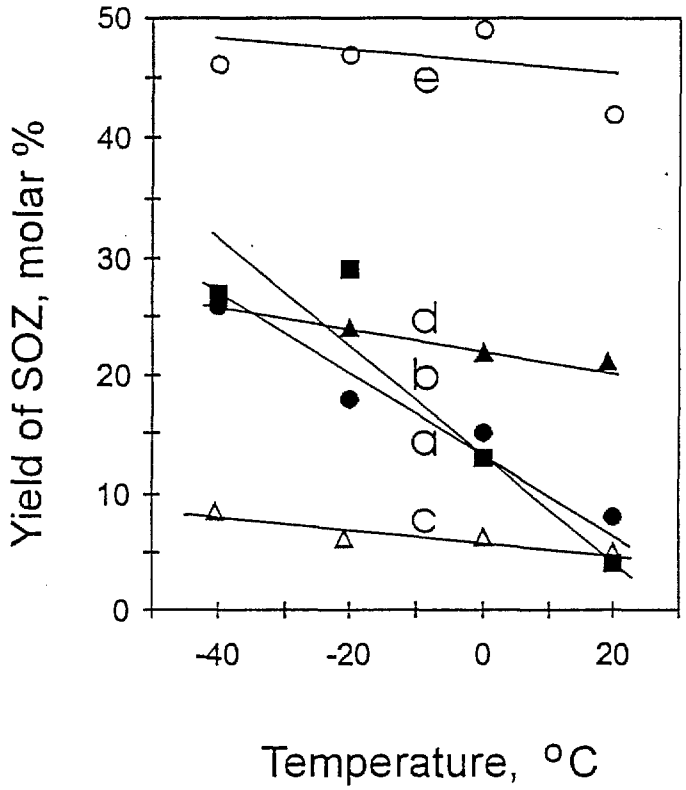
50
40
30
20
10
0
-40
-20
0
20
Yield of SOZ, molar %
Temperature, °C
e
d
b
a
c

FIG 6

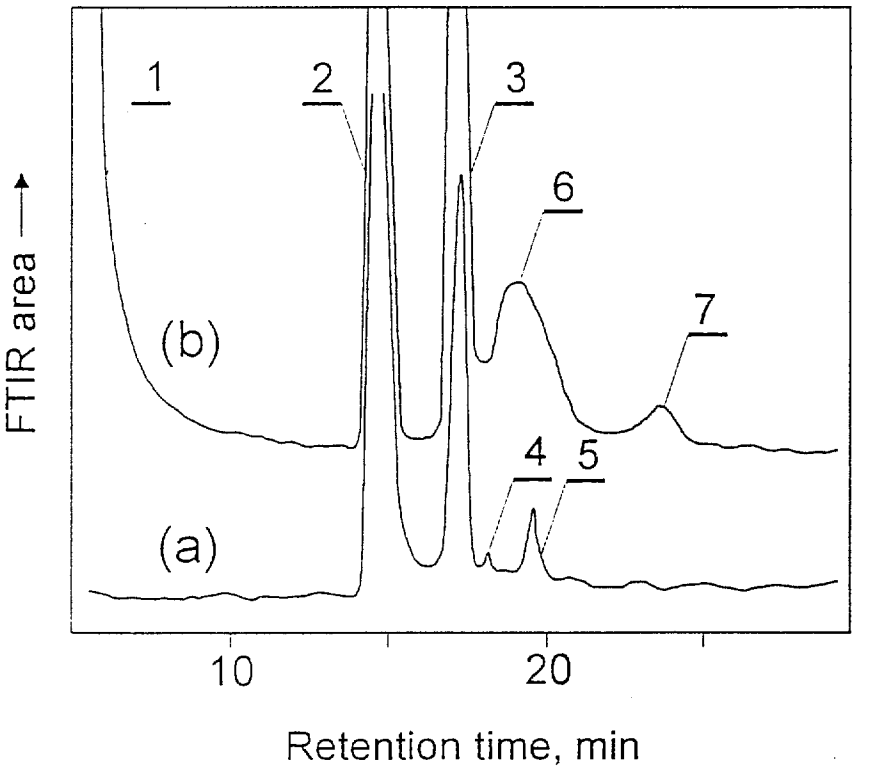

FIG 7

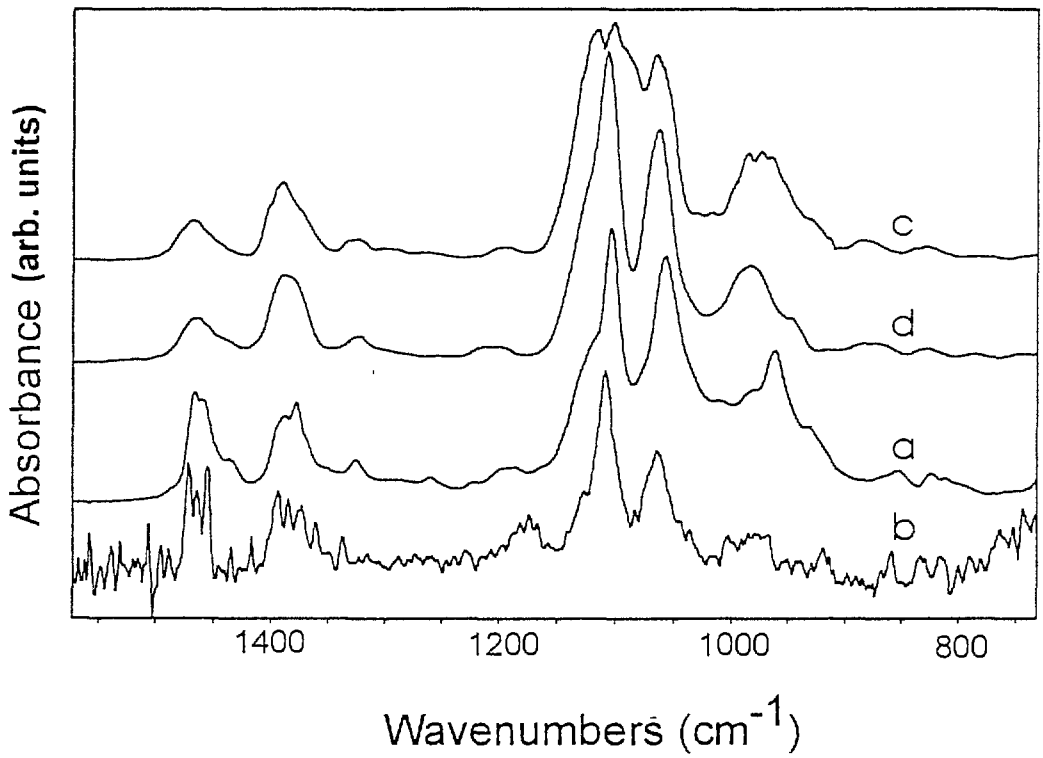
Absorbance (arb. units)
c
d
a
b
1400
1200
1000
800
Wavenumbers (cm-1)

FIG 8

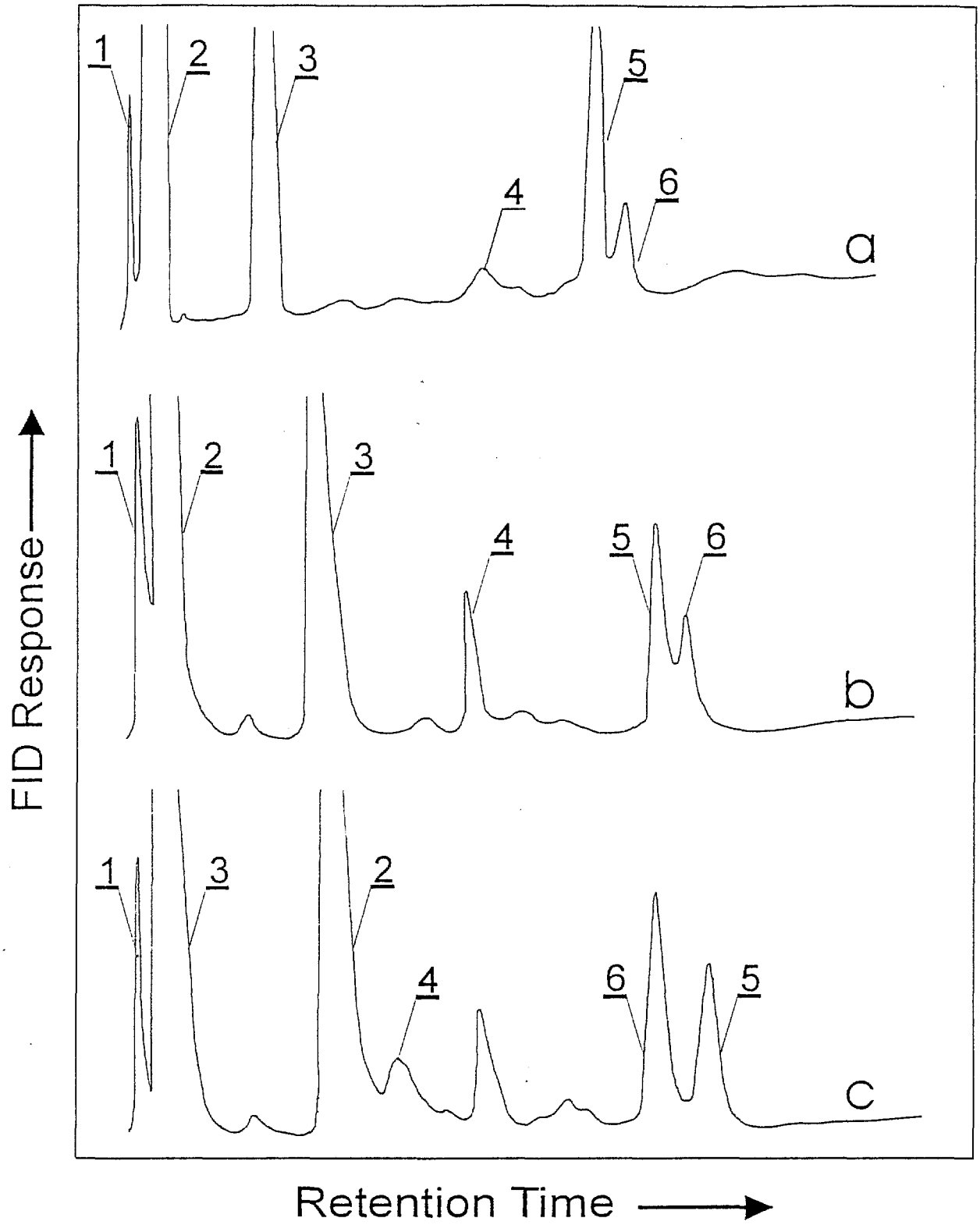

FIG 9

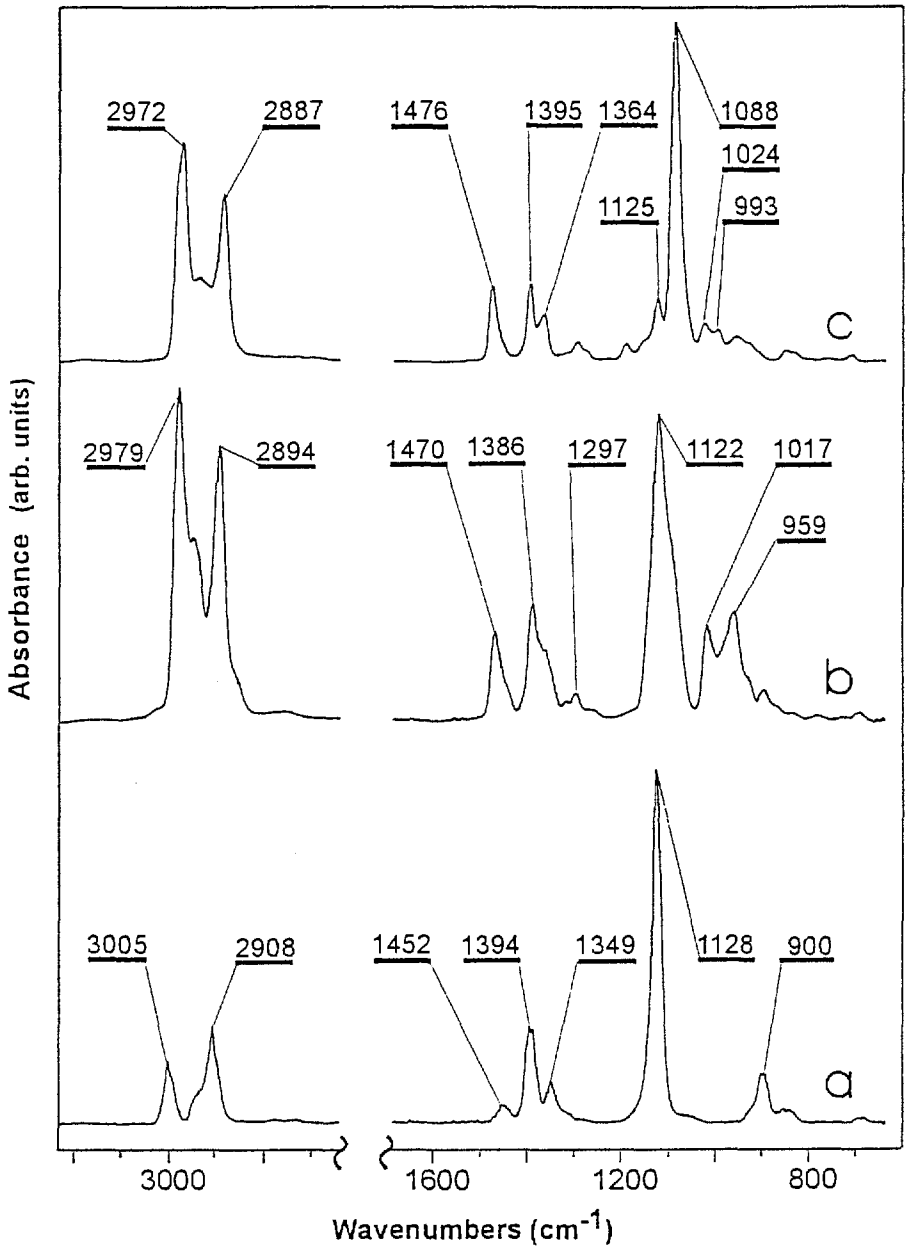
2972
2887
1476
1395
1364
1088
1024
1125
993
c
2979
2894
1470
1386
1297
1122
1017
959
b
3005
2908
1452
1394
1349
1128
900
a
Absorbance (arb. units)
3000
1600
1200
800
Wavenumbers (cm-1)

FIG 10

Table 1. IR and Mass Spectral Data of Standard SOZs.

SOZ	FTIR Spectrum cm^{-1}, rel.absorbance	Mass Spectrum (70 eV) m/z(rel.intensity,%)	
		Eight most intense peaks	The highest peak
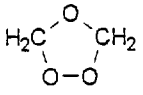	948,0.45; 955,0.45; 968,0.46; 1082,100; 1092,0.80; 2887,0.39; 2897,0.74; 2908,0.36; 2956,0.11; 2970,0.47; 2984,0.26	29(100); 30(92); 28(74); 46(67); 45(52); 44(31); 18(16); 76(10);	76(M+),10
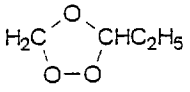	967,0,39; 973,0,42; 984,0,41; 1066,0,76; 1103,0,87; 1117,0,85; 1391,0,29; 1470,0,15; 2894,1,00; 2963,0,50; 2980,0,193	29(100); 27(38); 28(36); 31(23); 30(17); 57(12); 26(12); 75(10);	104(M+), 1.2
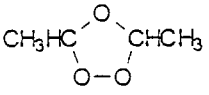	900,0.14; 1128,1.00; 1349,0.12; 1386,0.27; 1394,0.28; 1452,0.05; 2908,0.28; 3005,0.18;	43(100); 45(41); 44(34); 29(34); 89(16); 15(15); 60(11); 31(10);	104(M+), 5.0
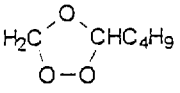	984,0.26; 1065,0.62; 1107,0.82; 1209,0.04; 1325,0.07;1390.0.24; 1466,0.12; 2890,0.85; 2967,1,00	29(100);44(60); 41(57); 27(41); 28(26); 43(25); 39(23); 57(23);	104(M-28), 0.8
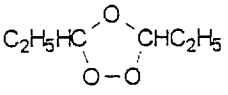	896,0.09; 959,0.33; 1017,0.29; 1122,0.92; 1297,0.09; 1386,0.35; 1470,0.27; 2894,0.83; 2950,0.55; 2979,1,00;	29(100); 57(43); 28(33); 58(31); 27(27); 31(23); 103(17); 41(11);	132(M+), 1.5
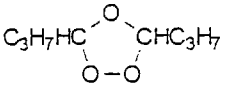	957,0.07; 993,0.09; 1024,0.11; 1088,1,00; 1125,0.19; 1191,0.06; 1294,0.06; 1364,0.14; 1395,0.23; 1476,0.23; 2887,0.50; 2938,0.25 2972,0.65;	43(100); 41(26); 27(17); 29(10); 72(8); 73(7); 39(7); 55(7);	117(M-C3H7), 0.9
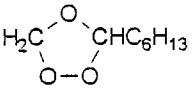	2953,1.00; 2855,0.82; 1463,0.35; 1395,0.28; 1380,0.34; 1325,0.16; 1225,0.09; 1200,0.12; 1103,0.91; 1057,0.82; 963,0.49;	43(100); 41(62); 29(56); 44(47); 55(45); 70(35); 57(29); 45(27);	132(M-28), 1.4

Table 2. SOZ trans/cis ratio

Olefin	Temperature / °C			
	20	0	-20	-40
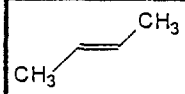	2,32	2,51	2,25	2,32
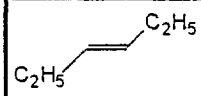	2,31	1,55	1,23	1,46
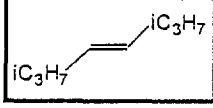	1,30	1,30	1,47	1,83

J. Mol. Struct. in press.

C12-223

MATRIX EFFECTS IN THE LOW TEMPERATURE OZONATION OF ETHYLENE, TETRAMETHYLETHYLENE AND 1-HEXENE

U. Samuni, Y. Haas*
Department of Physical Chemistry and the Farkas Center for Light-Induced Processes
The Hebrew University of Jerusalem, Jerusalem, Israel
R. Fajgar and J. Pola
Institute for Chemical Processes Fundamentals
The Czech Academy of Sciences
Prague, Czech Republic

ABSTRACT

The ozonnation of the title compounds was studied in argon and CO_2 matrices at low temperatures (12-80 K). All three were found to react with ozone in a CO_2 matrix deposited at low temperature, and having an amorphous structure. The reaction was found to start at 26 K, the temperature at which the matrix undergoes a phase transition. In contrast, only tetramethylethylene (TME) was found to react in an argon matrix, the other two compounds remaining inactive towards ozone up to the softening temperature of argon (~40 K). These results are interpreted as indicating that reaction between olefins and ozone is initiated at low temperatures once the two reactants are free to move to the required configuration. This idea is supported by molecular dynamics simulations on the TME reaction. The infrared spectra of the primary ozonide of TME, as well as of the primary and secondary ozonide of 1-hexene are reported, and compared with quantum chemical calculations.

1 INTRODUCTION

The Criegee mechanism [1, 2] is generally accepted as the best way to account for the characteristics of the ozonolysis of olefins, which leads to the cleavage of the double bond and the formation of aldehydes (or ketones) and acids. The three step mechanism involves three intermediates, the primary ozonide, I (POZ), a carbonyl oxide (CO) + carbonyl compound, II, sometimes referred to as the Criegee intermediate (C.I.) and the secondary ozonide, III (SOZ) (**Scheme 1**).

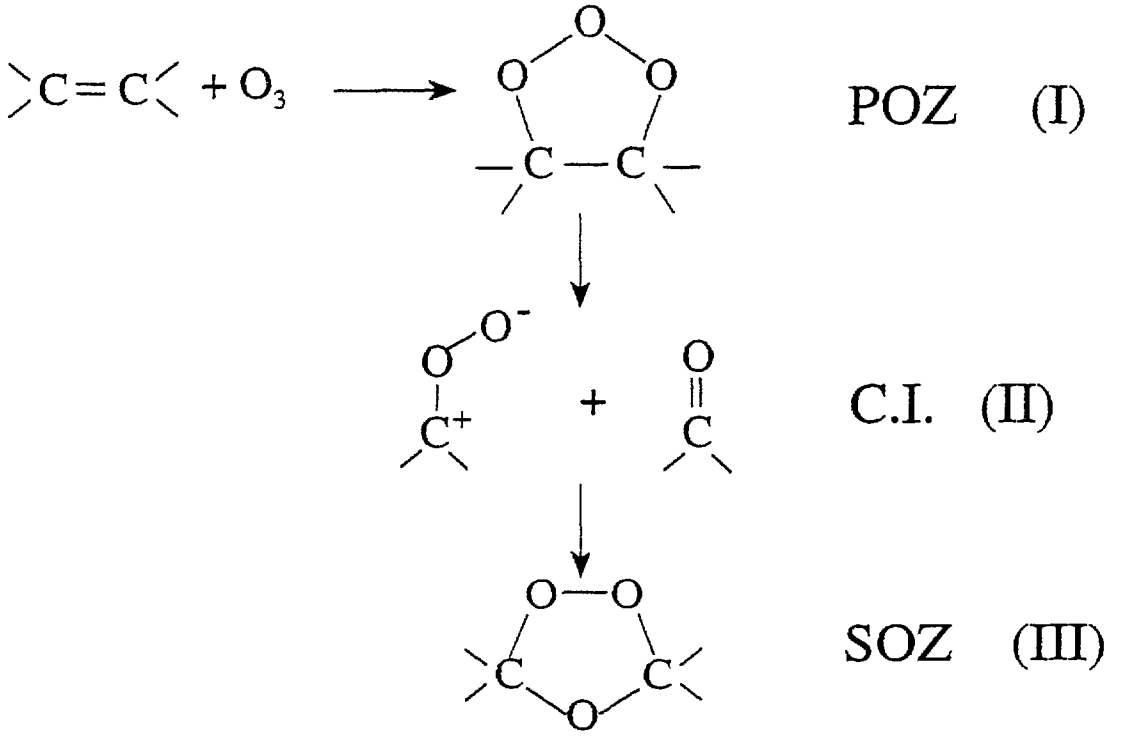

Scheme 1.

Recently, Cremer et al. calculated that a dipole complex should be formed between the CO and the carbonyl compound [3], this was further supported by our semiempirical calculations and comparison with experimentally found trends of ozonolysis steroselectivity of various olefins [4]. In a recent communication [5] we reported that

REC'D IN R&D/R
JAN 1 5

the primary and secondary ozonides of ethylene can be formed at much lower temperatures than previously observed, and that at a given temperature the reaction's progress depends on the matrix surrounding the reacting pair. Thus, no reaction was found to take place in an argon matrix at temperatures up to 44 K, or in a crystalline CO_2 below 77 K, while in an amorphous CO_2 matrix reaction products were identified at temperatures as low as 26 K. Molecular dynamics (MD) simulations of the trapping sites of the ethylene-ozone pair in an argon matrix were reported, and it was shown that their structure is unsuitable for ozonide formation. It was postulated that the apparently more open structure [6] of low temperature deposited CO_2 (T_{dep}=20 K), compared with the structure of crystalline CO_2 deposited at high temperature (T_{dep}=65 K) or to that of an argon matrix, allows the reaction to proceed at a lower temperature. However, a thermal reaction at a temperature as low as 26 K is difficult to explain in view of an estimated activation energy of 4.7-5.2 kcal/mol [7-9], for the ozonation reaction of ethylene in the gas phase and in solution. In addition, the study of ethylene ozonation at cryogenic temperatures [5] has revealed that the appearance of the two ozonide products, ethylene primary ozonide (EPOZ) and ethylene secondary ozonide (ESOZ), occurs simultaneously. Since at cryogenic temperatures EPOZ is very stable, this result was rationalized by assuming that ESOZ is formed directly from a vibrationally excited EPOZ molecule, before the latter undergoes relaxation. [5].

In this paper we extend the low temperature study (in argon and CO_2 matrices) to two C_6 olefins - tetramethylethylene (TME) and 1-hexene, in an attempt to check the generality of our previous findings - the very low reaction temperature (26 K) , the coappearance of EPOZ and ESOZ and better understand the environment effects on the reaction.

The room temperature reaction rate constants of larger olefins with ozone are bigger (e. g. by a factor of 1000 for TME) than of ethylene [9]. It is found experimentally that upon increasing chain length (for the 1-alkenes), and more importantly, the number of substituents on the double bond, the activation energy decreases (see **Table 1**).

Table 1. Kinetic data for ozonolysis of various olefins.

Olefin	A[a] cm^3 $molecule^{-1}s^{-1}$	Ea[a] kcal/mol	k_{uni} at 26 K[b] s^{-1}	$\tau_{1/2}$[c] s
ethylene	$1.2x10^{-14}$	5.2	$2.4x10^{-36}$	$2.9x10^{+35}$
1-propene	$1.3x10^{-14}$	4.2	$6.5x10^{-28}$	$1.1x10^{+27}$
1-butene	$3.46x10^{-15}$	3.4	$9.3x10^{-22}$	$7.5x10^{+20}$
cis-2-butene	$3.5x10^{-15}$	1.9	$3.8x10^{-09}$	$1.8x10^{+8}$
trans-2- butene	$9x10^{-15}$	2.3	$4.2x10^{-12}$	$1.7x10^{+11}$
2-methyl-butene	$6.2x10^{-15}$	1.6	$2.2x10^{-6}$	$3.1x10^{+5}$
TME	$3.7x10^{-15}$	0.7	$4.9x10^{1}$	$1.4x10^{-2}$

a. The bimolecular pre-exponential factor and the activation energy for the rate constants of the ozonolysis of olefins [9].
b. The unimolecular rate constants at 26K were computed by multiplying the bimolecular one by the concentration of ozone in a neat film consisting of a 1:1 composition of ozone and ethylene - $1.01x10^{22}$ molecule/cm^3.
c. $\tau_{1/2}$ =ln2/k.

In a cryogenic matrix diffusion is arrested, so that a reaction is possible only between neighboring reactants (a pair) formed during deposition. A measure of the time needed to experimentally observe a reaction may be obtained by considering the half life ($\tau_{1/2}$) of the reaction between such pairs. Table 1 shows the pseudo first order rate constants at 26 K, calculated from the high temperature parameters by assuming an effective ozone concentration of 10 M, corresponding approximately to a 1:1 ozone-olefin mixture, as well as the corresponding half lives. It is found that the reaction of TME may take place at a lower temperature range (20-40 K) during a typical experimental time interval (~10^4 s). In this temperature range the argon matrix is still intact, thus enabling to probe the effect of the argon environment. Activation data for 1-hexene ozonolysis are not available, but extrapolation from those of the smaller olefins indicates that this reaction may also be detected over a practical time interval (~10^5 s). In contrast, the reaction with ethylene is expected to be extremely slow and practically unobservable, if the room temperature rate parameters are valid also at cryogenic temperatures. In particular the reaction onset is expected to be observable at a different temperature for ethylene than for TME in cryogenic matrices.

TME ozonolysis was studied by various techniques and in different phases. In neat films Heicklen et al. identified TMEPOZ bands at T≥183 K [10]. Nelander et al. studied TME and ozone in argon and in crystalline CO_2 matrices (CO_2 matrices deposited at a temperature of 65 K) [11]. In this study, relatively high concentrations (1:1:100) were used - so that the possible involvement of complexes larger than 1:1 in the reaction cannot be neglected. These workers searched for a charge transfer UV absorption band in these systems,

but failed to observe any. In contrast, the more recent work of Singmaster and Pimentel, in which a careful control of the temperature was exercised, reported a charge transfer complex of TME - ozone using visible-UV absorption in krypton and argon matrices [12]. Several low temperature gas phase studies attempted to map out the product distribution for TME (and also 1-hexene) ozonolysis, in an effort to clarify the complete reaction mechanism [13-16].

1-Hexene ozonides were studied by Razumovskii et al. and later on by Boldenkov, the activation energy for ozonide decomposition was determined: 7 kcal/mol (±20%) [17] for the primary ozonide (HPOZ) and 23.7 kcal/mol [18] for the secondary ozonide (HSOZ). Later on, Mile et al. investigated the infrared spectra and kinetics of decomposition of 1-hexene primary ozonide in the liquid phase at low temperatures ($\log_{10}A=-3$ sec^{-1}, Ea<2.9 kcal/mol) [19], which is different from the value reported by Razumovskii.

In 1-hexene low temperature ozonation both HPOZ and HSOZ were observed, a trend typical of primary olefins [5, 20]. In contrast, low temperature TME ozonation yields only the TMEPOZ which dissociates to the final end products at higher temperatures. The absence of TMESOZ was accounted for within the framework of the Criegee mechanism by assuming that the ketone formed from TMEPOZ is inert towards reaction with the carbonyl oxide, preventing the retrocycloaddition step and TMESOZ formation [10, 20, 21]. Recently Griesbaum et al. have succeeded synthesizing TMESOZ by the indirect method of ozonation of O-methyl oxime of acetone and later detected TMESOZ (though in minute amounts) in the ozonolysis of TME on polyethylene. They found that TMESOZ is a very stable molecule and characterized it by NMR, IR and CI-MS spectroscopies[22, 23].

Previous cryogenic studies of the ozonolysis reactions were aimed mostly at identifying reactive intermediates and did not explicitly consider the effect of site structure - possible environmental influence on the reaction's feasibility and progress rate. In particular the high concentration of reactants used may have led to reactions within large reactant's clusters, perhaps obscuring matrix effects. In this study, an effort was made to work with the highest dilution that still enabled the detection of products, thus, contrary to the majority of previous matrix studies, making it easier to follow the specific role of different matrix environments. In this paper we report experiments designed to assess influence of the solid environment on the reaction feasibility and progress as well as preliminary attempts to correlate the data with computer simulations of site structure.

2. EXPERIMENTAL AND COMPUTATIONAL DETAILS

Ozone was prepared from a purified oxygen (98.5%, main impurity N_2) by electric discharge. Ethylene (99.5%) from Aldrich, 1-hexene (99%) from Aldrich, tetramethylethylene (TME) (98%) from Fluka, Argon (99.9999%) from Matheson, CO_2 (99.6%) from Gordon-Gas, were all used as received. Each gas was mixed separately with a carrier gas (argon or CO_2) to the desired concentration using standard manometric techniques. The gases were co-deposited (at a rate of 2-10 mmol/hour) from two different gas lines on a KBr window attached to the cold tip of a closed cycle helium cryostat (Air Products model CS202). A stainless steel line was used for the olefins and an all-glass vacuum line was used for ozone, to reduce ozone decomposition during deposition. The infrared spectrum of the resulting matrix was recorded by a Fourier transform spectrometer (Nicolet model 520, 0.5 cm^{-1} resolution) at any desired temperature higher than 12 K. The temperature was controlled by a Lake Shore Cryogenics Temperature Controller (model 330 Autotuning) to within ±0.5 K. Three characteristic temperatures were used in the experiments: T_{dep}, the deposition temperature, T_{reac}, the reaction temperature, and T_{spec}, the temperature at which the spectrum were recorded. Typically the matrix temperature was raised gradually, the temperature at which new product bands first appeared in the IR spectra is refered to as T_{reac}. The matrix was left at the reaction temperature for periods varying between a few minutes and several hours.

Amorphous CO_2 matrices were prepared by using T_{dep}=20 K or lower. It was claimed that for CO_2 [24-26], deposition in the temperature range of 15-30 K leads to the formation of an amorphous solid, while careful deposition at temperatures higher than 55 K results in a cubic T_{6h} crystalline structure. The amorphous form is characterized by the appearance of "forbidden" molecular transitions of CO_2, ν_+ and ν_- (1384.5 and 1279 cm^{-1} respectively), which are believed to be induced in the solid by a non symmetric structure [24-26]. Under these deposition conditions the resultant solid has a very high surface area as determined from H_2 absorption [6, 27] experiments. It should be noted that minor impurities in the CO_2 gas may be important to the formation of the amorphous matrix; Thus, Knozinger et al. [6] reported, based on X-ray powder diffraction, the formation of polycrystalline CO_2 matrix when using ultra clean (99.995%) CO_2 gas even at low deposition temperature, 20 K (though, at these conditions they also reported a high specific surface area, 210 m^2/g and in addition the X-ray technique is only sensitive to ordered structure). Depositions in mixed solvent were done by pre-mixing CO_2 and argon to the desired ratio; all other deposition conditions (such as deposition temperature and deposition rate) were the same as those used to generate the amorphous neat CO_2 matrix.

In all experiments, the appearance and subsequent growth of new bands in the infrared spectrum was the indication that reaction took place. The assignment of the spectra was aided by an ab-initio calculation of the vibrational frequencies and infrared intensities of the relevant POZ and SOZ products. Ab-initio calculations were carried out using the Gaussian 94 (and Gaussian 92) program package [28], at the HF or HF-MP2 levels

53

and by the density functional theory at the B3LYP level. Several basis sets were used, the largest of which was 6-311G* [29]. Complete structural optimization was performed for each species and vibrational frequencies were calculated from the Hessian matrix using the harmonic approximation at the optimized geometry. No imaginary frequencies were found in the calculation, showing that the optimized structure was indeed a minimum. The resulting frequencies were uniformly scaled for the HF-MP2/6-31G calculation by 0.9338 or 0.9613 for the B3LYP/6-311G* [30].

Molecular dynamics simulations were performed as previously described [31], except that the molecules were treated as rigid bodies using the RATTLE algorithm [32]. The geometry of the molecules used in the MD simulations was taken either from microwave experimental data or, when these were not available such as for TMEPOZ, from ab initio calculations (MP2/6-31G for TMEPOZ). Different trapping sites could be generated in different runs, and the most frequently encountered ones were considered the most stable ones, as discussed in more detail elsewhere [31].

3. RESULTS

3.1 Ozonation in low temperature deposited CO_2 matrices:

1-Hexene and ozone were found to react in an amorphous CO_2 matrix at temperatures as low as 26 K. **Figure 1** shows a portion of the IR spectra of 1-hexene and ozone in an amorphous CO_2 matrix. Warming the matrix to 26 K brought about a decrease of the ozone and 1-hexene bands and the appearance of new bands. These bands belong to HPOZ and HSOZ based on literature data [19], on our neat film results and supported by ab initio calculations (see Tables 2 and 3). After 2 hours at 26 K, there was further decrease in the reactants bands and increase of the products bands.

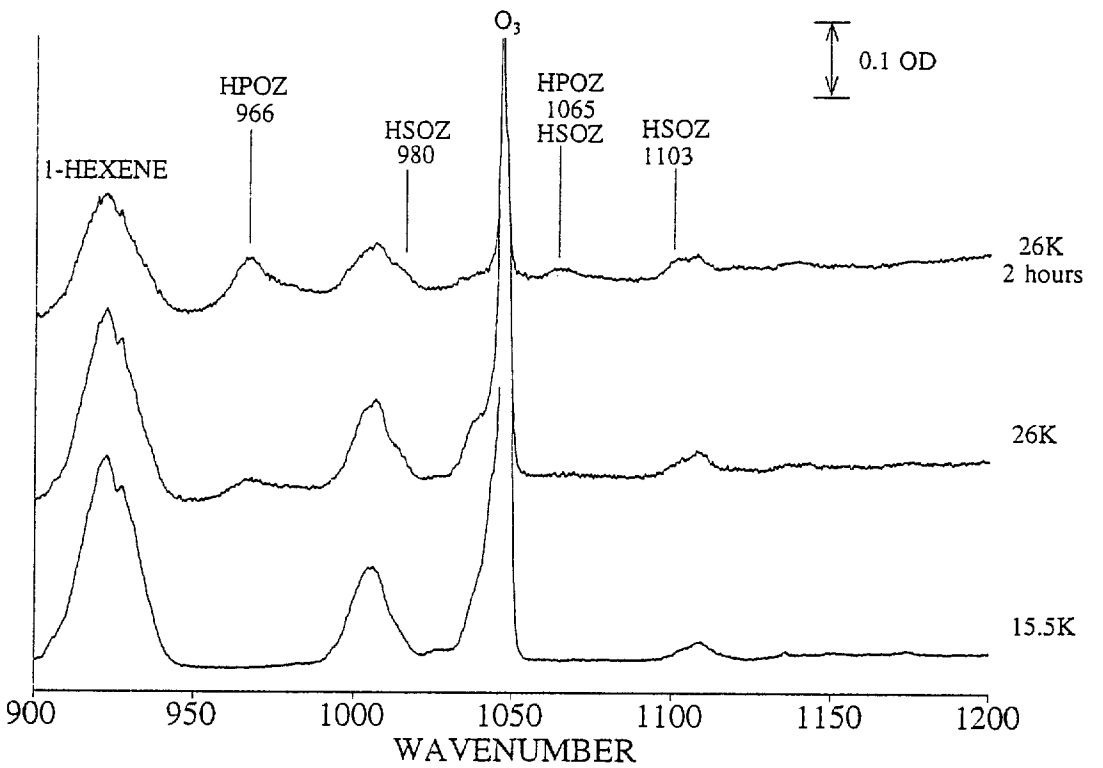

Figure 1. IR spectra of 1-hexene and ozone in an amorphous CO_2 matrix (1-hexene:ozone:CO_2 1:1:700; T_{dep}=15.5K) Bottom: Just after deposition at 15.5K. Middle: After heating the matrix to 26K. Top: After 2 hours at 26K.

TME and ozone deposited in an amorphous CO_2 matrix (T_{dep}=12.5 K) did not react at temperatures lower than 25-26 K. At that temperature new bands assignable to TMEPOZ [10] appeared and continued to increase reaching a plateau after 14 hours (**Figure 2**).

For both olefins, (as was the case with ethylene ozonation [5] *no* IR bands due to either POZ or SOZ were observed, even for elongated periods of time (several days), as long as the matrix was kept at temperatures below 25 K.

54

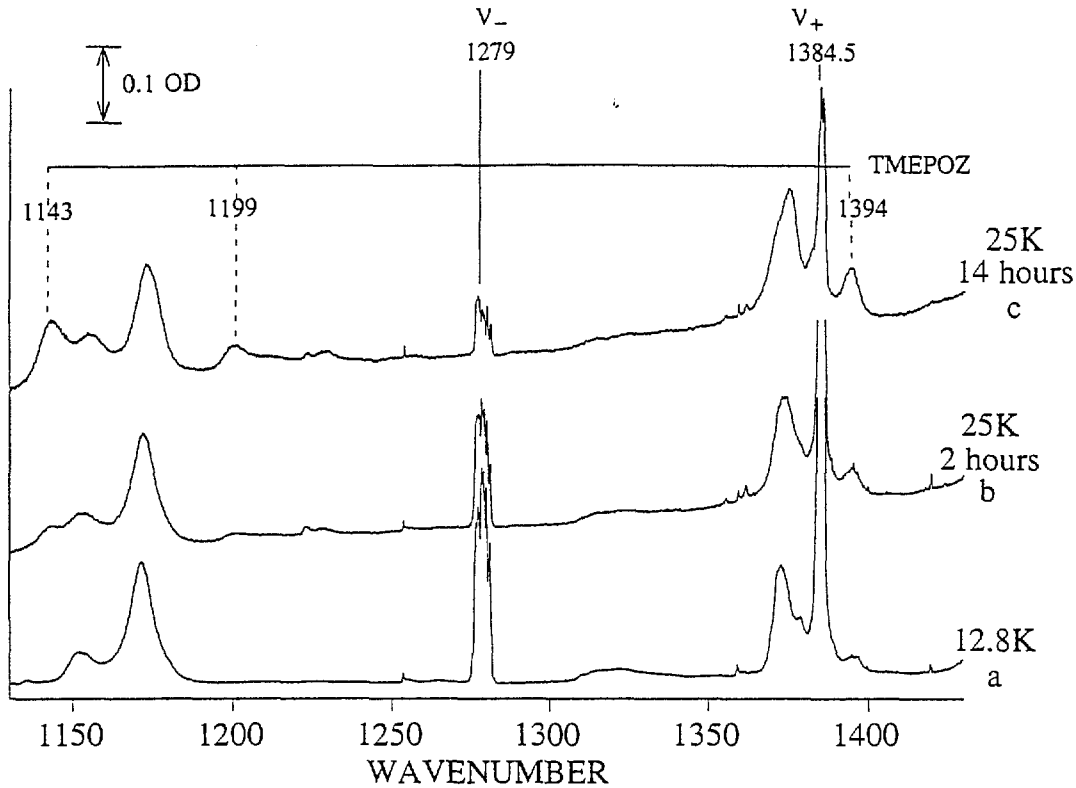

Figure 2. IR spectra of TME and ozone in an amorphous CO_2 matrix (TME:ozone:CO_2 1:1:620; T_{dep}=12.8K) a. Just after deposition at 12.8K. b. After 2 hours at 25K. c. After 14 hours at 25K.

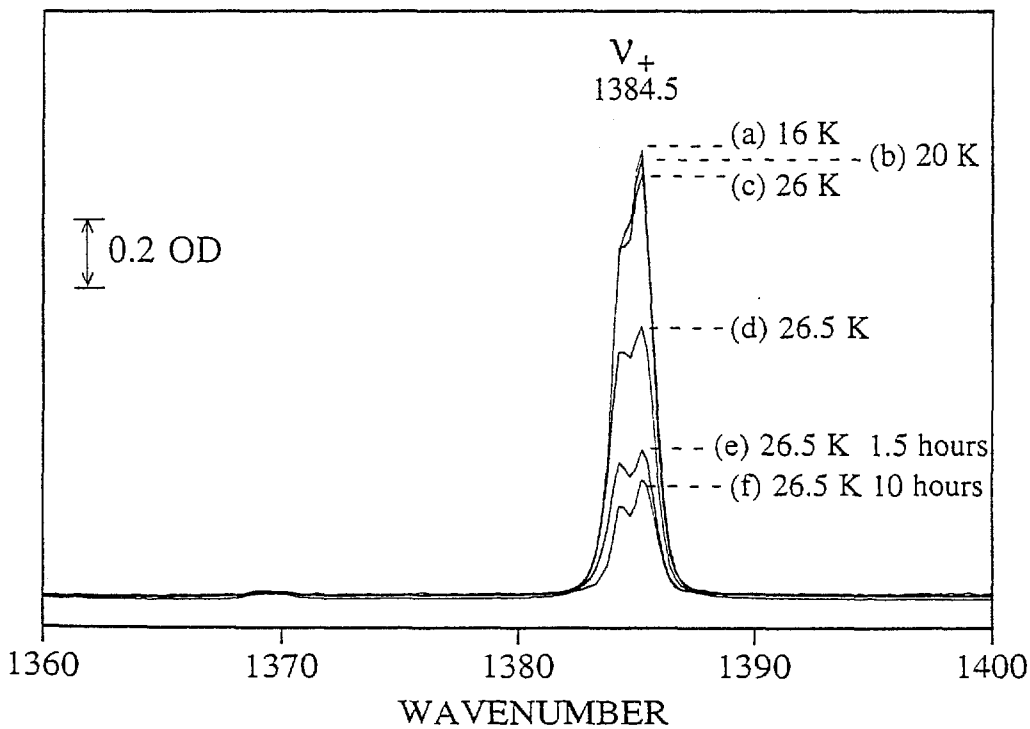

Figure 3. IR spectra of a low temperature deposited CO_2 matrix (O_3:CO_2 1:310 T_{dep}=15K) a. Just after deposition at 15.5K. b. At 20K. c. Just after heating to 26K. d. At 26.5, 30 minutes from first warming to 26K. e. After 1.5 hours at 26.5K. f. After 10 hours at 26.5K.

3.2 CO_2 matrix crystallization process:

Another significant change that occurred during heating of the low temperature deposited CO_2 matrix is the decrease of the CO_2 ν_+ and ν_- bands (1384.5 and 1279 cm^{-1} respectively) [24-26]. This decrease is clearly seen

55

in figure 2. It was observed for all low temperature deposited CO_2 matrices, even when only one component (or none) was introduced to the matrix. We noted that in all these matrices the changes started only at the temperature range of 25-26 K.

Figure 3 demonstrates this for an amorphous CO_2 matrix containing only ozone as a guest, namely, when ozonation does not take place. It can be seen that below 26 K there is a negligible decrease of the molecular "forbidden" bands of CO_2 (ν_+, ν_-), but upon heating to 26.5 K a rapid decrease sets in: within 30 minutes the peak's area decreased by 30%.

3.3 Ozonation in argon matrices:

TME and ozone reacted in an argon matrix at temperatures as low as 30 K. **Figure 4** shows a portion of the IR spectrum of TME and ozone in an argon matrix. Examination of the lowest trace, taken just after deposition (at T=12.5 K), shows that it already contains weak bands of TMEPOZ probably due to some reaction during deposition. Raising the matrix temperature up to 30 K does not lead to any detectable spectral changes. At that temperature a gradual increase of TMEPOZ bands and a decrease of the TME bands is clearly observable. The matrix was maintained at the same temperature for elongated periods of time, until the product bands intensity reached a constant value. In this matrix, raising the temperature further (for instance to 35 K) yielded an *additional* increase in the product bands intensity (see figure 4), showing that the plateau reached at the lower temperature did not represent complete exhaustion of the reaction potential in the matrix under diffusion-limited conditions. At 40 K a sharp increase of the product bands (and a decrease of those of the reactants) is observed. At this temperature the argon matrix softens, and translational motion of trapped species becomes possible. This finding is in accord with the report of Nelander et al. of TME ozonation in an argon matrix upon heating to 40 K [11].

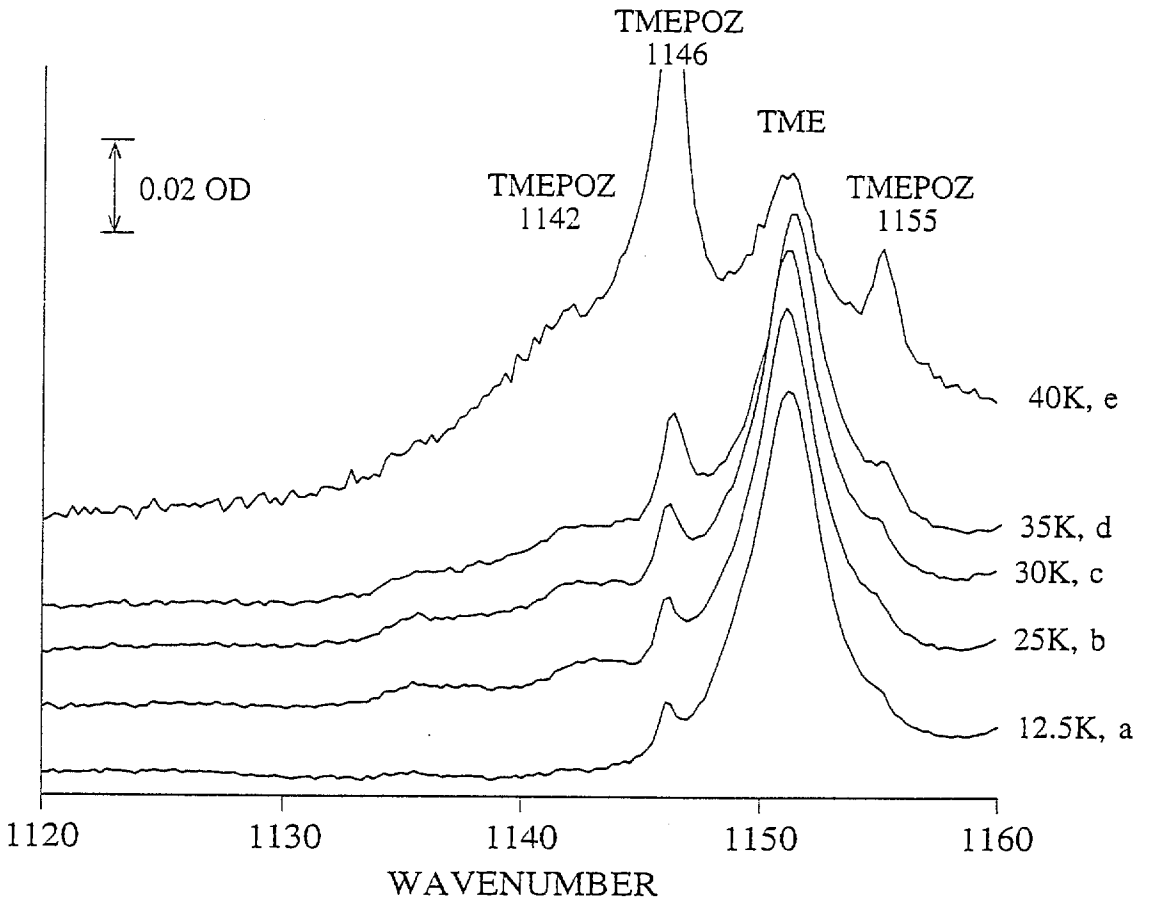

Figure 4. IR spectra of TME and ozone in an argon matrix (TME:ozone:Ar 1:1:650; T_{dep}=12.5K) a. Just after deposition at 12.5K. b. After 11.5 hours at 25K. c. After 7 hours at 30K d. After 30 minutes at 35K e. After 40 minutes at 40K.

In contrast with the above TME results, no reaction between 1-hexene and ozone in an argon matrix could be detected below 40 K. When the temperature was raised above 44 K product bands appeared conspicuously (as in

56

the case of ethylene [5]). At this temperature the vapor pressure of argon is high enough for the matrix to be quickly pumped away, and the infrared spectra of the remaining species was found to contain a mixture or unreacted reactants (1-hexene and ozone) and of the HPOZ and HSOZ, as determined by comparison with previously published spectra [19] and ab initio calculated frequencies (see Tables 2 and 3).

3.4 Ozonation of a 1:1 mixture of ethylene and TME in amorphous CO_2 matrix:

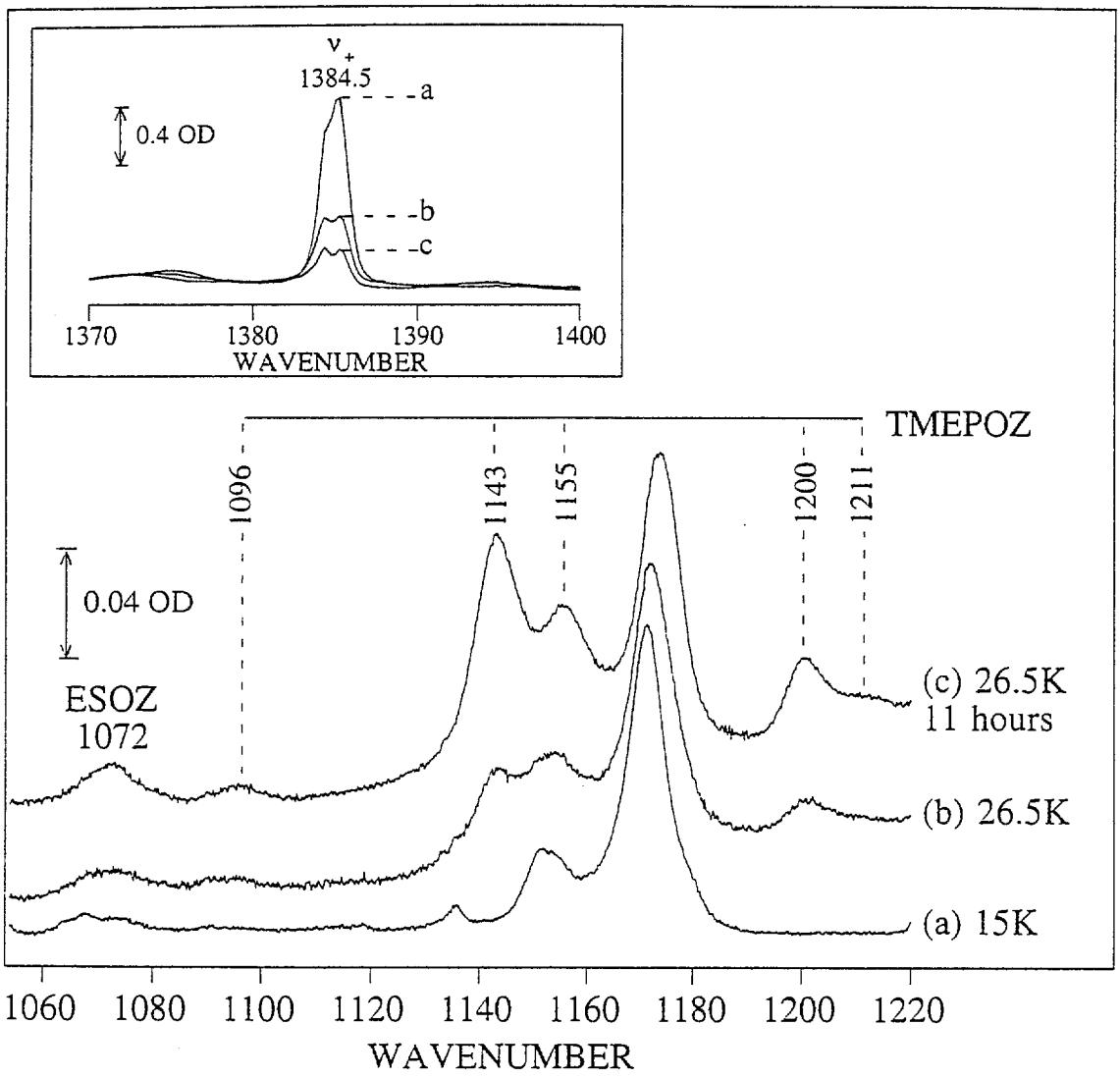

Figure 5. IR spectra of TME, ethylene and ozone in a amorphous CO_2 matrix (TME:ethylene:ozone:CO_2 1:1.12:2:600; T_{dep}=15K) a. Just after deposition at 15K. b. Just after heating to 26.5K. c. After 11 hours at 26.5K. The insert shows the change in the ν_+ CO_2 band, under the same conditions.

Figure 5 shows a portion of the IR spectra of a codeposition of TME and ethylene with ozone in a CO_2 amorphous matrix. Upon warming the matrix to 26 K new bands assignable to both ethylene ozonides and TMEPOZ appear. Warming to a lower temperature than 26 K did not bring about any increase of TME ozonation products bands in spite of its lower gas phase activation energy (compared to ethylene ozonolysis, see Table 1). Rather, both TME and ethylene ozonides first appear only at 26 K.

Figure 6 compares the rate of formation of TMEPOZ and ethylene SOZ at 26.5 K in a CO_2 amorphous matrix (TME:ethylene:ozone:CO_2 1:1.12:2:600) by monitoring the area of their strongest bands (1143 cm^{-1} for TMEPOZ and 1072 cm^{-1} for ESOZ). In order to convert the values from optical density to concentration one needs the molar extinction coefficients (the initial concentration of reactants being the same and the optical path-length being identical since both are in the same matrix). Unfortunately, these coefficients are not available. A rough estimate of the extinction coefficients ratio was obtained from an ab initio calculation (MP2/6-31G) of the vibrational frequencies and IR intensities of these ozonides: 30 and 170 km/mole for the two bands, respectively. Thus, optical densities were converted to concentrations by dividing the experimental OD by the calculated IR

intensity. The validity of this estimate was checked by comparing the TMEPOZ concentration determined from two different TMEPOZ IR bands: 1143 and 1200 cm^{-1}: the resulting concentration were equal to within 10% (the area of the 1200 cm^{-1} band was divided by a calculated IR intensity of 6 km/mole). The resulting changes in relative concentrations with time are shown in Figure 6. It is found that at 26.5 K the TMEPOZ's rate of formation is much faster than that of ESOZ (by a factor of ~30). Note that the matrix was kept at 25 K for about 2 hours before beginning the 26.5 K experiment, resulting in the appearance of weak product absorption bands, which account for the finite product concentration at time zero in Figure 6.

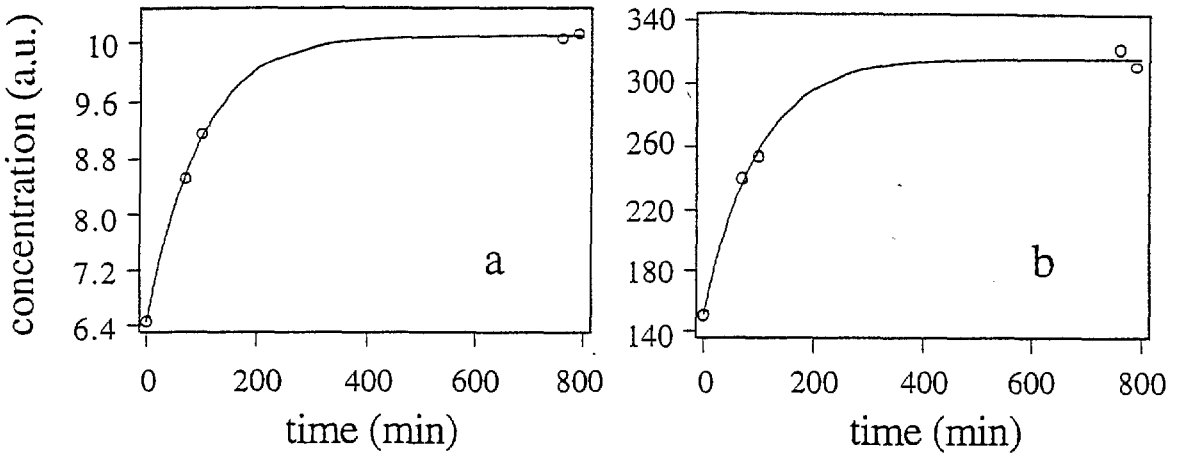

Figure 6. The rate of formation of TMEPOZ and ESOZ at 26.5K in a CO_2 amorphous matrix (TME:ethylene:ozone:CO_2 1:1.12:2:600). See text for the method used to convert IR intensities to concentrations. a. ESOZ (1072 cm^{-1} band), b. TMEPOZ (1143 cm^{-1} band). The curves are calculated assuming pseudo first order kinetics, yielding the rate constants listed in Table 2. The fit quality was good: R^2=0.999 and 0.995 respectively.

The calculated curves shown in Figure 6 assume pseudo first order kinetics. For the two curves shown in the Figure, the rate constant is found to be $(1.05 \pm 0.08) \times 10^{-2}$ min^{-1}. It follows that while the rate of formation of TMEPOZ is much larger than that of ESOZ, the *rate constants* of the reactions are practically identical. Converting these rate constants back to a bimolecular rate constant, using an effective ozone concentration of 10 M as in Table 1, we get $k=2.8 \cdot 10^{-25}$ $cm \cdot molecule \cdot s^{-1}$, eleven orders of magnitude *smaller* than the rate extrapolated from the high temperature data for ethylene, and twenty six orders of magnitude *larger* than the rate extrapolated from the high temperature data for TME. **Table 2** compares the pseudo first order rate constants for ethylene or TME ozonation in several separate experiments. It can be seen that although there is some scatter in the data all values are similar, within an order of magnitude, and there is no obvious trend with temperature or olefin indicating that within the experimental error the rate constants are the same. In conclusion, even though the number of data points in Figure 6 is too small for an accurate determination of the rate constants, evidently the simple extrapolation from the high temperature rate parameters obtained in fluid media is not appropriate.

Table 2. Rate constants of ethylene and TME ozonide formation in amorphous CO_2 matrix.

Exp.	Matrix composition	Ozonide	IR Band cm^{-1}	Temperature K	k_{uni} min^{-1}
1	ethylene:ozone:CO_2 1:1:580	ESOZ	1072	25	$(1.4 \pm 0.6) \times 10^{-3}$
2	ethylene:ozone:CO_2 1:1:580	ESOZ	1072	26.5	$(2.6 \pm 0.8) \times 10^{-3}$
3	TME:ethylene:ozone:CO_2 1:1.12:2:600	ESOZ	1072[a]	26.5	$(1.06 \pm 0.03) \times 10^{-2}$
3	TME:ethylene:ozone:CO_2 1:1.12:2:600	TMEPOZ	1143[b]	26.5	$(1.05 \pm 0.08) \times 10^{-2}$
3	TME:ethylene:ozone:CO_2 1:1.12:2:600	TMEPOZ	1200	26.5	$(8.1 \pm 0.5) \times 10^{-3}$
4	TME:ozone:CO_2 1:1:620	TMEPOZ	1200	25	$(3.9 \pm 0.4) \times 10^{-3}$

a. See figure 6a.
b. See figure 6b.

3.5 Ozonation of ethylene in mixed matrices:

The fact that the reaction is observed in amorphous CO_2 at temperatures as low as 25-26 K suggests the use of this porous 'solvent' for the quantitative study of the kinetics of reactions characterized by low activation barriers. Quantitative estimates of the rates in amorphous CO_2 were hampered by its tendency to be fragile under the conventional preparation scheme used in this work. In an attempt to prepare a mechanically more stable matrix while maintaining the low temperature reaction, mixed matrices were made up of CO_2 and argon in varying proportions. In most of these experiments the olefin used was ethylene.

It was found that the location and shape of the reactants (ethylene and ozone) IR bands strongly depended on the matrix composition.

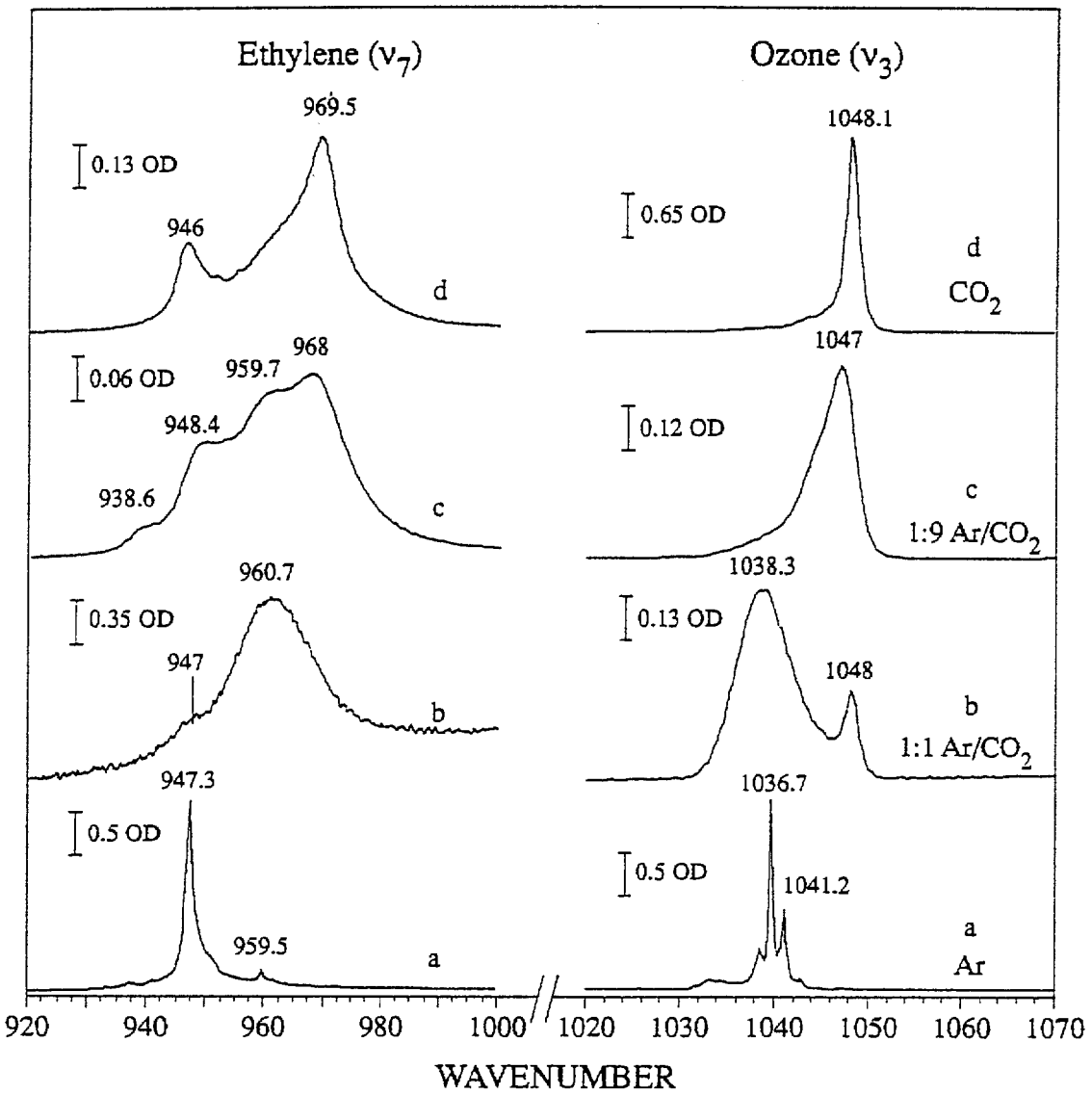

Figure 7. The IR spectra in the region of ethylene's ν_7 band and ozone's ν_3 band in different matrix compositions. a. ethylene:ozone:argon 1:1:630, T_{dep}=15K; b. ethylene:ozone:solvent 1:5:2000, solvent mixture is Ar:CO_2 1:1, T_{dep}=18K; c. ethylene:ozone:solvent 1:1:700, solvent mixture is Ar:CO_2 1:9, T_{dep}=17K; d. left side is ethylene:CO_2 1:280, T_{dep}=15K; right side is ozone:CO_2 1:300, T_{dep}=20K.

Figure 7 shows the IR spectra in the region of the ν_7 band of ethylene (left side) and the ν_3 band of ozone (right side) in different matrices. The ozone ν_3 band was centered at 1039.7 cm^{-1} in argon and at 1048.1 cm^{-1} in the CO_2. The ethylene ν_7 band was at 947.3 cm^{-1} in argon and at 969.5 and 946 cm^{-1} in the CO_2 matrices. The "forbidden" CO_2 molecular bands, ν_+ and ν_-, were observed in all of the prepared mixed matrices. When the CO_2 content was less than 90%, no reaction was observed even upon heating up to 35 K and leaving the matrix overnight. Upon warming the 1:9 Ar/CO_2 mixture (ethylene:O_3:solvent 1:1:700) to 26 K the ν_+ and ν_- lines decreased and new product bands appeared and increased with time (**Figure 8**).

59

Again it is noted that both processes begin only at 26 K and not at a lower temperature. In the 1:1 $Ar:CO_2$ (O3 dilution 1:400 ethylene dilution 1:1800) mixed matrix the ν_+ and ν_- lines are also present, however they remain unchanged at 26 K. Moreover, no new product bands could be detected (heating to 32 K and maintaining the matrix at that temperature overnight also lead to no decrease of the ν_+ and ν- lines nor to any product formation). Attempts to induce a reaction between ozone and 1-hexene in mixed matrices (8:2 $Ar:CO_2$ and 9:1 $Ar:CO_2$) in the 26-35 K temperature also did not lead to product formation.

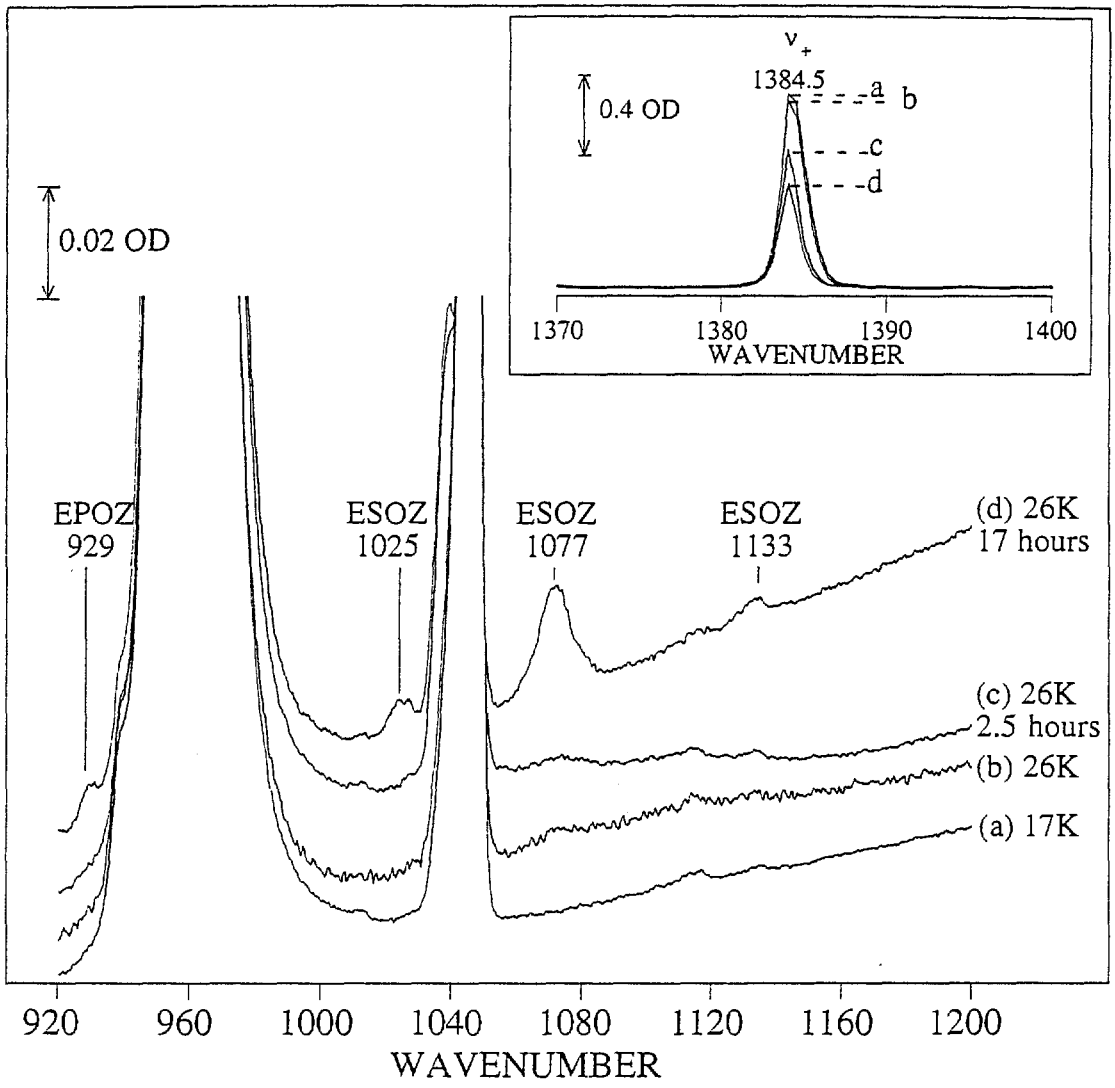

Figure 8. IR spectra of ethylene and ozone in a low temperature deposited mixed matrix (dilution ethylene:ozone:solvent 1:1:700; solvent mixture is: $Ar:CO_2$ 1:9 ; T_{dep}=17K) a. Just after deposition at 17K. b. Just after heating to 26K. c. After 2.5 hours at 26K d. After the 17 hours at 26K. The insert shows the spectral region of the "forbidden" CO_2 molecular transitions, ν_+/ν_-.

4. DATA ANALYSIS

4.1 Vibrational spectra of the product ozonides

4.1.1 HPOZ and HSOZ bands in a neat film

The infrared spectra of HPOZ and HSOZ were recorded in a neat film experiments. Bands due to a given species were assigned by monitoring the rate of their increase and then decrease as a function of time at the following temperatures: 120 K, 150 K, 170 K, 180 K and 220 K. At these temperatures the reactants 1-hexene and ozone evaporate and thus ambiguity in the assignment due to overlap with the product bands is eliminated.

Figure 9 shows the IR spectra of a 1-hexene and ozone mixture in an argon matrix just after deposition at 15 K and then at increasingly higher temperatures the gradual disappearance of the reactant bands (due to reaction and evaporation), the appearance of product bands (primarily HPOZ) at 120 K and 150 K and finally at 170 K the disappearance of HPOZ bands and increase of HSOZ bands.

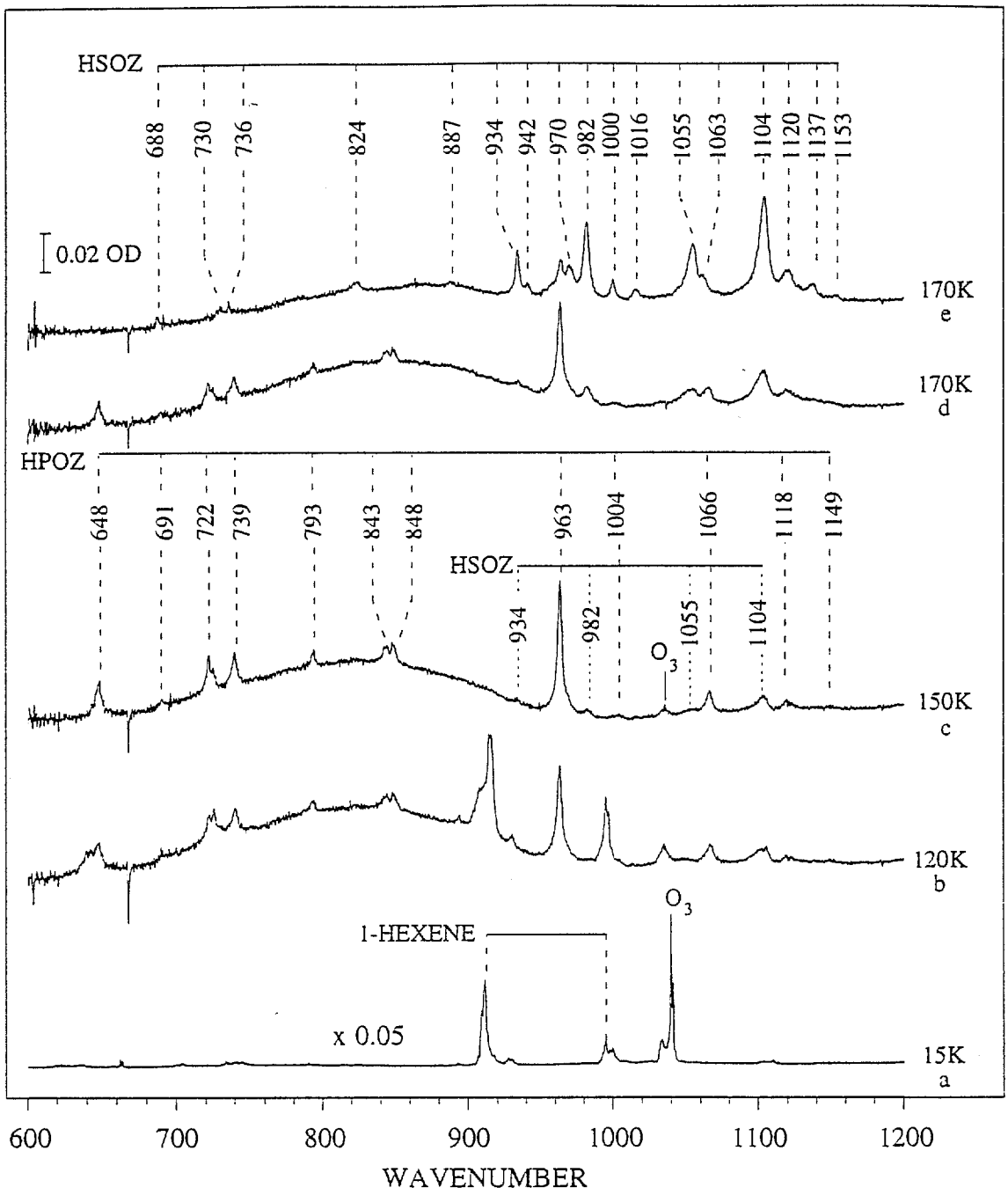

Figure 9. IR spectra of 1-hexene:ozone:Ar 1.5:1:815 matrix a. Just after deposition at 15K ; b. After 1 hour at 120K; c. Just after heating to 150K; d. Just after heating to 170K; e. After 3.7 hours at 170K. (Spectra b-e are in a neat film since the argon solvent has evaporated).

To assist in the product bands assignment we performed ab initio calculations of HPOZ and HSOZ vibrational frequencies. **Table 3** shows a comparison of experimental and calculated vibrational frequencies of HPOZ. The tentative assignment (in the absence of any isotopic data) was helped by considering both the calculated frequency and IR intensities. Agreement between calculated and experimental frequencies is seen to be reasonably good. Calculations were performed at different levels of theory, the most extensive ones being MP2-6-311G* and B3LYP/6-311G*.

These calculations yielded also the optimized geometry of HPOZ, for which experimental data are not yet available. The structure obtained by a DFT (B3LYP/6-311G*) calculation, shown in **Scheme 2** indicates that the five membered ring (COOOC) is nearly of C_S symmetry, similar to the experimentally reported one for EPOZ [33] which was also by obtained computationally [34].

61

Table 3. The experimental and calculated vibrational frequencies of HPOZ.

Exp. frequency[a] cm^{-1}	Exp. freqency[b] neat film cm^{-1}	Exp. intensity.[b] neat film arbitrary units	Calc. frequency.[c] cm^{-1}	Calc. intensity[c] km/mol
692	648	30	668	7.2
	691	3	688	3.9
725	722	29	704	15.8
740	739	26	713	21.9
	793	9	771	2.2
	843	15	826	2.8
	848	15	868	3.8
			882	2.5
			905	2.5
975	963	100	946	39.5
			975	0.3
			982	0.9
1001	1004	4	999	1.3
			1025	0.5
	1066	16	1052	4.0
	1118	6	1105	3.2
	1149	1	1141	0.4
			1191	0.3
	1208	2	1211	1.0
1230	1227	8	1238	0.9
	1235	3	1272	0.2
1275	1274	5	1288	0.7
			1298	0.2
	1316	3	1305	2.8
	1334	4	1322	1.4
	1372	18	1353	8.4
			1361	2.2
	1389	5	1375	4.7
			1441	0.7
			1446	1.1
			1457	1.4
			1460	8.7
			1462	1.1
	1470	133	1469	9.9
	2841	5	2886	9.2
	2858	93	2899	25.8
			2906	0.4
	2871	49	2908	18.6
	2895	7	2909	37.6
	2913	20	2917	38.6
			2928	17.5
	2929	131	2931	56.9
			2955	30.9
	2949	127	2967	93.2
	2967	75	2972	47.4
			2995	28.1

a. Experimental vibrational frequencies [19].
b. Experimental vibrational frequencies in a neat film - this work. Intensity determined from the area of the vibrational bands in a neat film, and normalized to the strongest band in the finger print region. Note that the 1470 cm^{-1} band is wide, corresponding to several calculated frequencies (in the region 1460-1470) which explains the seemingly mismatch of intensities. In addition the bands in the 2800-3000 cm^{-1} region of the experimental spectra are broad and overlaping causing siginifcant uncertainty in the determination of the area of individual bands.
c. Calculated vibrational frequencies, (B3LYP/6-311G*, factor of 0.9613).

62

Table 4. The experimental and calculated vibrational frequencies of HSOZ.

Exp. freqency[a] gas phase cm^{-1}	Intensity[a] arb. units	Exp. Frequency[b] neat film cm^{-1}	Intensity[b] arb. units	Calc. frequency[c] cm^{-1}	Intensity arb. units
		688	3	704	1.1
		730	5	711	2.9
		736	2	733	1.8
				772	6.8
		824	7	823	8.4
				846	4.5
		887	3	867	11.9
				894	3.3
		934	20	947	18.4
		942	6	967	58.6
		970	17	984	3.2
984	32	982	44	1023	45.0
		1000	8	1026	3.2
		1016	5		
1065	76	1055	43	1073	184.7
		1063	11		
1107	100	1104	100	1092	34.6
		1120	27	1118	9.2
		1137	11	1129	5.9
		1153	1	1192	2.3
1209	5	1208	6	1203	1.9
		1220	8	1227	0.4
		1249	4	1264	3.9
		1287	3	1280	1.5
				1298	1.0
				1311	1.0
				1354	7.8
1325	9	1340	8	1359	25.8
1390	29	1379	19	1367	12.4
		1400	4	1374	13.9
		1414	1	1437	4.0
				1446	0.5
				1457	0.7
				1459	8.9
1466	15	1470	72	1470	10.0
				1476	1.0
2890	104	2861	59	2887	8.3
		2871	26	2896	38.0
		2928	195	2902	107.0
				2908	38.1
				2914	12.4
				2918	26.4
				2932	23.3
				2942	13.1
				2964	6.4
2967	122	2955	193	2968	115.0
				2969	56.0
				2998	21.0

a. Experimental vibrational frequencies in the gas phase [16], intensities normalized to the strongest band at the finger print region (1107 cm^{-1}).
b. Experimental vibrational frequencies in a neat film - this work. Intensities determined from the area of the vibrational bands in a neat film, and normalized to the strongest band in the finger print area. Similar to the HPOZ results, Table 3, the bands in the 2800-3000 cm^{-1} region of the experimental spectra are wide and overlap causing siginifcant uncertainty in the determination of the area of individual bands.
c. Calculated vibrational frequencies, (B3LYP/6-311G*, factor of 0.9613).

63

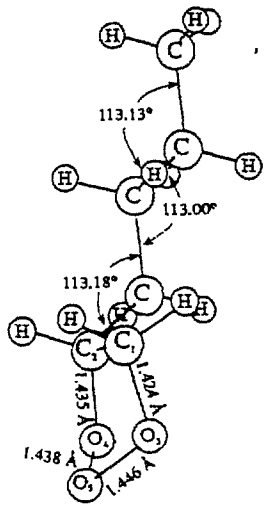

HPOZ CALCULATED GEOMETRY
SIDE VIEW

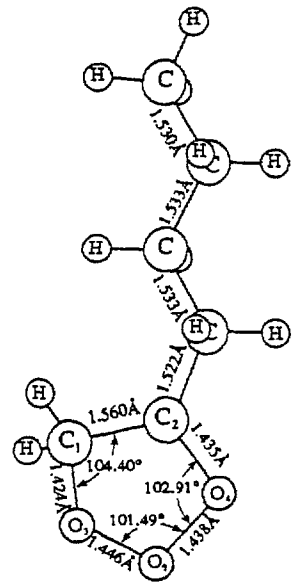

HPOZ CALCULATED GEOMETRY
TOP VIEW

Scheme 2.

Table 4 shows that the experimental spectrum of HSOZ also agrees well with the calculated one. **Scheme 3** shows the calculated geometry of HSOZ (B3LYP/6-311G*). The structure of the five membered ring (COOCO) is nearly of C_2 symmetry, similar to that reported for ESOZ, as found experimentally [35, 36] and in calculations [34]. The calculations thus support the notion that the ozonides of primary olefins (i.e. having a terminal CH_2 group) have a similar ring structure as ethylene ozonides.

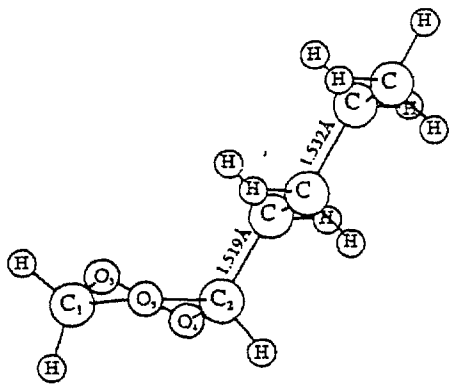

HSOZ CALCULATED GEOMETRY
SIDE VIEW

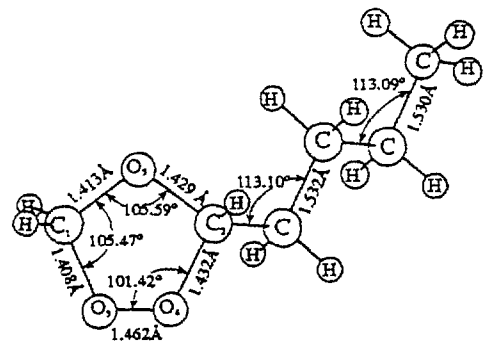

HSOZ CALCULATED GEOMETRY
TOP VIEW

Scheme 3

4.1.2 TME ozonide bands

The IR spectra of TMEPOZ were recorded in an argon matrix (**Table 5**), a CO_2 matrix and in a neat film. The peaks were assigned to a given single chemical species by monitoring their simultaneous change with time as a function of temperature. None of the peaks that appeared in matrices containing TME and ozone, or upon TMEPOZ decomposition could be identified with the TMESOZ frequencies reported by Griesbaum et al [23] or with those obtained by our ab initio calculations (see **Table 6**). Thus, TMESOZ is not formed in argon or CO_2 matrices nor in a neat film.

Table 5. The experimental and calculated vibrational frequencies of TMEPOZ.

Exp. frequency[a] cm^{-1}	Exp. frequency[b] cm^{-1}	Exp. intensity[b] arb. units	Calc. frequency[c] cm^{-1}	Calc. intensity[c] km/mol
	576	2	576	4.33
	650	12	611	0.43
	668	1	635	12.09
682	691	15	674	5.38
721	729	100	757	11.28
	843	9	790	8.85
852	854	25	880	1.47
953	950	10	924	0.43
			926	0.22
			927	0.35
			993	0.25
	1095	6	1003	0.11
	1142	35	1136	14.22
1148	1146	95	1149	27.40
	1152	27	1164	30.47
1197	1196	25	1193	6.15
			1219	0.20
	1261	8	1249	1.90
			1368	2.71
1370	1394	28	1370	22.89
			1382	16.76
			1390	6.98
			1448	0.83
			1452	2.47
			1454	9.64
			1463	1.69
			1470	7.49
			1473	10.13
			1477	5.69
	1482	8	1482	10.67
			2866	1.93
			2867	5.98
			2869	16.73
			2871	20.41
			2944	2.60
			2945	2.04
			2949	35.79
			2950	21.41
			2974	2.83
			2975	10.99
			2976	2.20
			2976	21.18

a. Experimental vibrational frequencies in a neat film at 88K [10].

b. In an argon matrix, at 37K. Intensities are derived from the area of each peak. Note that at the 2800-3000 cm^{-1} region TMEPOZ bands are overlapped by TME bands.

c. Calculated vibrational frequencies (MP2/6-31G, factor of 0.9338).

65

Table 6. The experimental and calculated vibrational frequencies of TMESOZ.

Exp. frequency[a]	Exp. intensity[a]	Calc. frequency[b]	Calc. intensity[b]
cm^{-1}	arb. units	cm^{-1}	km/mol
845	0.4	821	10.6
860	0.2	827	30.6
876	0.3	868	0.3
		898	2.7
		901	0.8
		932	0.8
1005	1.0	971	117.7
		977	0.5
		978	0.2
1115	0.2	1094	8.3
1215	1.4	1180	253.7
		1191	1.9
1245	0.6	1192	48.4
1265	0.3	1213	69.7
		1233	5.9
		1355	0.9
1375	0.9	1357	59.5
		1368	30.9
		1372	2.5
		1432	0.0
		1435	0.0
		1436	2.7
		1448	0.5
		1434	0.7
		1453	0.1
		1455	1.8
1470	0.2	1461	16.5
		2926	0.0
		2926	22.6
2940	0.4	2933	25.9
		2934	0.9
		2989	9.4
		2989	5.0
		3000	9.8
3000	0.6	3000	48.3
		3009	4.5
		3010	32.3
		3013	37.6
		3013	1.7

a. Experimental vibrational frequencies [23]. Intensity was estimated from a transmitance spectra [23].
b. Calculated vibrational frequencies, (B3LYP/6-311G*, factor of 0.9613).

As in the case of HSOZ and ESOZ, TMESOZ calculated geometry is found to be of C_2 symmetry (see **Scheme 4**). However, TMEPOZ geometry is calculated to be of C_2 rather than C_s symmetry found for primary ozonides (**Scheme 5**). The twisting of the five member ring (COOCO) to a C_2 symmetry helps to minimize the repulsion between the four methyl groups, as can be seen from the side view. **Table 7** lists the geometry, dipole moment, rotational constants, calculated geometry, and energy of TMEPOZ calculated, using several methods and basis sets. The main difference between the simple HF calculation and the more extensive MP2/4-31G and MP2/6-31G ones involved the O-O-O ring. This result is expected since a proper description of the O-O-O moiety should include correlation effects. Interestingly, the AM1 calculation resulted in TMEPOZ of C_s geometry, similar to that of EPOZ. Other main differences of this calculation (compared to the rest of the calculations) are in the O-O-O angle (by 4°) and in the O-O bond (by -0.28 Å). To verify that TMEPOZ equilibrium geometry is indeed of C_2 rather than C_s symmetry, the calculation was repeated (using high level methods and large basis sets) starting with the AM1 optimized geometry of TMEPOZ (of C_s symmetry). In all instances the calculation's optimization procedure lead to a final geometry of C_2 symmetry.

66

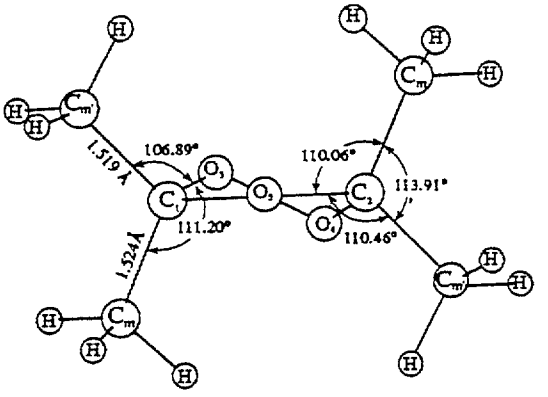

TMESOZ CALCULATED GEOMETRY
SIDE VIEW

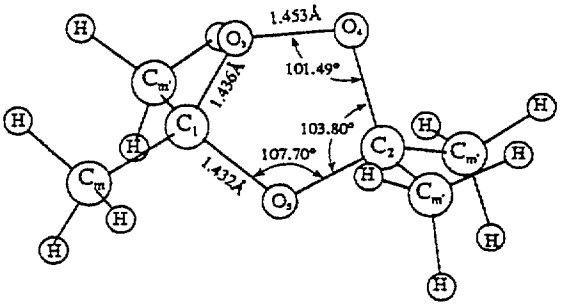

TMESOZ CALCULATED GEOMETRY
TOP VIEW

Scheme 4

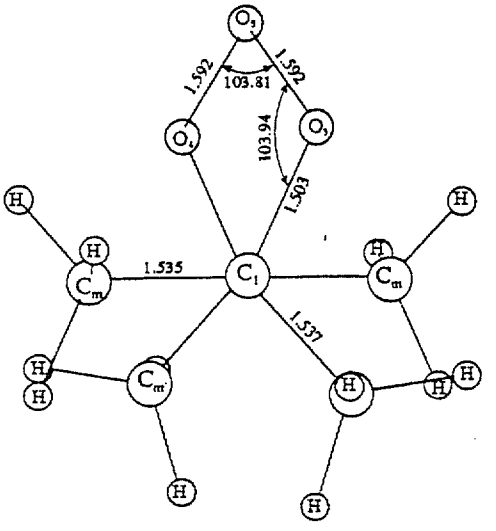

TMEPOZ CALCULATED GEOMETRY
SIDE VIEW

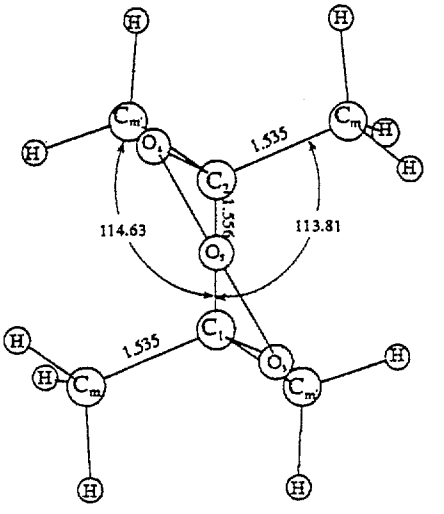

TMEPOZ CALCULATED GEOMETRY
TOP VIEW

Scheme 5

It is interesting to note that the calculations involving basis functions with polarization functions (such as 6-31G* or 6-311G*) failed to reach an optimized geometry for TMEPOZ, rather the frequency calculation reveal the calculated geometry to be a transition state (one imaginary frequency).

Table 8 summarizes and compares the calculated total energy, geometry (rotational constants) and dipole moment of the 4 different ozonides.

5. DISCUSSION

5.1 Comparison with ethylene ozonation:

The results of TME and 1-hexene ozonation in an amorphous CO_2 matrix are in good qualitative agreement with the previous findings for ethylene [5]. Both TME and 1-hexene react with ozone at a very low temperature (25-26 K) in amorphous CO_2. The appearance of the POZ and SOZ in the case of 1-hexene is simultaneous, as found for the ozonation of ethylene, thus, supporting the need to modify the Criegee mechanism as suggested in our previous work [5]. A possible explanation for the reactivity in the amorphous CO_2 (compared to the lack of reactivity, for ethylene and 1-hexene, in the argon matrix) is its considerably porous structure. Such a structure is likely to contain spacious trapping sites that do not hinder the molecular rearrangements required during the ozonation reaction, contrary to the restrictions imposed by the rigid trapping sites in an argon matrix [5]. However, this explanation does not account for the onset of the reaction at a very low temperature (26 K), considering the high gas phase activation energy (~5 kcal/mol for ethylene [9]). From Table 1 it is evident that at 26 K practically no reaction should be observable for ethylene and other small unbranched olefins (though it is feasible for TME). The reactivity of ethylene at 26 K could be explained were the activation energy in the matrix

lower than the gas phase one. However, since in *crystalline* CO_2 the reaction occurs only above 77 K, the lowering of the activation energy must be related not only to the chemical nature of CO_2 but also to the amorphous matrix structure. The amorphous matrix is known to be porous, having a very large surface area as found from H_2 absorption experiments [6, 27] which maximizes at deposition temperature of 20 K [27]. Thus it could be suggested that there may be a surface effect stabilizing the transition state that catalyzes the reaction, due to the unsymmetrical nature of a surface and to the large quadrupole moment of CO_2 (1.43×10^{-39} Å s m^2 [37]). However, no other examples of catalysis by a CO_2 solvent were reported, making this option extremely unlikely.

Table 7. The calculated dipole moment and geometry of TMEPOZ.

	MP2/6-31G	MP2/4-31G	AM1	HF/4-31G
Dipole moment (Debye)	5.24	5.20		5.04
Rotational Constatns (MHz)				
A	1825.50	1833.40	1948.74	1913.22
B	1723.59	1733.47	1760.01	1769.07
C	1451.48	1458.32	1509.20	1509.02
Bondlengths (Å)				
r (C_1-O_3)	1.503	1.500	1.480	1.464
r (C_1-C_2)	1.556	1.552	1.562	1.543
r (C_3-O_5)	1.592	1.591	1.303	1.469
r (C_m-C)	1.535	1.531	1.514	1.521
r ($C_{m'}$-O)	1.537	1.533	1.514	1.518
Bond angle (deg)				
$C_1C_2O_4$	101.62	101.58	100.64	100.27
$C_1O_3O_5$	103.94	103.76	107.99	106.35
$O_3O_5O_4$	103.81	103.80	108.05	105.78
$C_1C_2C_m$	113.81	113.84	114.61	113.83
$C_1C_2C_{m'}$	114.63	114.61	114.61	115.49
Dihedral angle (deg)				
$C_1O_3O_4C_2$	326.99	326.73	0.00	329.37
$C_mC_1C_2C_{m'}$	313.94	313.35	0.00[a]	317.06
Energy (h)	-459.3470558	-458.8867553		-457.9244513

* Atom numbering correspond to the geometry of TMEPOZ as depicted in scheme 5.

** C_m - stands for carbon of a methyl. Due to the symmetry of the molecule, of the four methyl groups there are only two types: C_m and $C_{m'}$.

a. For the AM1 calculated TMEPOZ which is of C_s symmetry the relevant angle for comparison is C_mCCC_m.

Table 8. Calculated properties of TME and 1-hexene primary and secondary ozonides.

Ozonide	HPOZ	HSOZ	TMEPOZ	TMESOZ
Level	B3LYP/6-311G*	B3LYP/6-311G*	MP2/6-31G	B3LYP/6-311G*
Energy (H)	-461.4653137	-461.5445300	-459.3470558	-461.5673947
Rot. Const. (MHz)				
A	5139.00	4502.82	1825.50	2719.92
B	618.72	679.62	1723.59	1386.66
C	580.87	646.73	1451.48	1260.63
Dipole Moment (Debye)	3.89	1.31	5.24	1.40

68

Another suggestion is that for specific reactions the activation energy in the matrix may be lower than in the gas phase one. Pimentel et al. [38, 39] examined the kinetics of the oxidation of NO to NO_2 by O_3 in nitrogen matrices. Even though the gas phase activation energy is at least 10 kJ/mol (2.4 kcal/mol) a reaction was found to occur at the temperature range 12-20 K (activation energy determined to be 443 J/mol). Furthermore, for the ozonation of cis-2-butene and trans-2-butene in a krypton matrix Pimentel and Singmaster [12] reported values for the activation energy which were on the low end range of the gas phase measured values. This led the authors to make the following statement: "That raises the interesting question of whether the gas-phase value is an average of all collision geometries whereas in the carefully prepared matrix all of the geometries are the same and that this preferred geometry happens to be optimum for the ozonolysis reactions." [12]. It is interesting to note that for the ozonation of ethylene the lower range value of the activation energy determined in a crystalline CO_2 matrix (3-5 kcal/mol) was again lower than the gas phase value (4.7 kcal/mol) [40, 7]. However, even a value of 3 kcal/mol seems too high to allow a reaction at 26 K. Moreover, Pimentel's suggestion calls for a carefully prepared matrix generating the optimal geometry for a reaction, whereas an amorphous CO_2 matrix is not likely to contain only one optimal site geometry but rather a distribution of sites.

Another possibility is that the activation energies derived for the ozonolysis reaction at high temperatures (Table 1 and reference [9]) are not relevant at cryogenic temperatures. When the activation energies are small (as is the case for the ozonolysis reaction) the assumption that temperature dependence of the pre-exponential factor in the Arrhenius expression is negligible is no longer valid. Thus, for a bimolecular reaction with zero activation energy, the gas kinetic collision frequency increases with the square root of the temperature, leading to a larger rate constant. In a limited temperature range, of say 280-370 K, this increase may be erroneously interpreted as an activation energy of ~2 kcal/mol. It is interesting to note that another olefin, trans-2-butene is also reported to react at cryogenic matrices already at 25 K [41], whereas if the high temperature derived activation energy (2.3 kcal/mol) is to be used a negligible rate constant is expected (Table 1). Similarly, 1-propene is reported in the same paper to react already at 50 K - a temperature much too low if the literature activation energy is to be used. These results support the notion that the high temperature Arrhenius parameters are not applicable at cryogenic temperatures.

It is proposed that the ozonation reaction at the low temperature of 26 K in amorphous CO_2 matrix is related to the phase transition (crystallization process). It is noted that in all cases where ozonation commenced in amorphous CO_2 matrices there was a concomitant decrease in the CO_2 "forbidden" molecular transitions (ν_+ and ν_-). This decrease is thought to originate from a crystallization process that the amorphous system undergoes in the temperature range of 25-55 K [24]. This effect was noted also in pure CO_2 solids when no reaction was involved (see figure 3). The connection between the reaction and the crystallization may not be coincidental. A previous study of solid CO_2 [27] noted that at low deposition temperatures (the effect maximizing at 20 K according to adsorption measurements) an increasing part of CO_2 molecules form a metastable phase, being extremely unstable against temperature perturbations. Under these conditions considerable amounts of energy (estimated as 1% of the condensation energy) were released upon structural changes (phase changes). It was postulated that this metastable phase is formed when the CO_2 molecules aligned with each other in parallel. This energy release, however, cannot be used to overcome the room temperature estimated barrier, as the following rough estimate shows. The condensation energy (which is equal to the enthalpy of evaporation) is 70 cal/g (3.08 kcal/mol) at -30°C [42]. If the crystallization energy released is indeed about 1%, it will amount to about 31 cal/mol. This is much too small for the ethylene reaction to take place unless some kind of energy pooling occurs.

The crystallization process is accompanied by structural changes that may reduce environmental structural restrictions on the reaction. Although it ultimately leads to the creation of a more organized and a more tightly stacked solid (a crystal), the formation of the CO_2 crystal may eject the ethylene-ozone pair out into spaces in between crystallites. Some experimental data seem to support this suggestion. In particular it rationalizes the fact that for *all* olefins studied (ethylene, 1-hexene, TME) the threshold temperature for a reaction in amorphous CO_2 was about 26 K, even though the activation energies that apply to these different olefins vary considerably. If the reaction is initiated by the crystallization process then indeed the threshold temperature should be independent of the nature of the olefin. Our experiments with pure amorphous CO_2 matrices (or with only one of the reactants) show that indeed the crystallization process starts at 26 K.

5.2 Mixed matrices:

The composition of mixed matrices was studied by various methods, including neutron inelastic scattering and X-ray diffraction, using both low mixing ratios (less than 5%) and up to complete mixing (a 1:1 mixture) [43-45]. Molecular dynamics based computer simulations helped to estimate the structure of these complex systems [46, 45]. Guests trapped in these matrices may be found either in an environment of one of the pure components (poor mixing) or in a site formed by both (strong mixing).

CO_2/Kr mixed matrices were studied recently by X-ray diffraction and IR [45], showing that using regular codeposition from the gas phase, phase separation occurred, presumably by diffusion during deposition. A homogeneously mixed solid of CO_2 and Kr formed only upon increasing the cooling efficiency during

69

deposition by using a helium flow. In the concentration range of 30-70 mol% Kr the resultant solid was amorphous. MD simulations support this finding and imply that it is due to internal distortions (orientational and center of gravity disorder) rather than to grain size effects [45].

The nature of the Ar/CO_2 mixed matrices prepared in this work (homogenous mixture or phase separation) was probed by considering changes in the IR spectrum of ozone and ethylene. In the 1:1 Ar/CO_2 mixture two IR bands due to the ν_3 ozone mode were found: a dominant one having the typical frequency of ozone in pure argon matrix (1038.3 cm^{-1}) and the smaller one (about 1/7 in area) having the typical frequency of ozone in a pure CO_2 matrix (see figure 7). This may imply that the resultant matrix is predominantly composed of two separate phases, with the ozone concentrated mostly in the argon one. The relatively large width of the ozone bands indicates that this separation is not complete, but some minor mixing between the phases does occur. The spectrum of ethylene in the 1:1 Ar/CO_2 mixture also shows one major band and one minor band (960.7 and 947 cm^{-1} respectively, see figure 7). The latter is the same as ethylene's band in argon, indicating that a small part of the ethylene resides in a pure argon phase. (This is also the frequency of the minor band of ethylene in a CO_2 matrix but the frequency of the stronger band the 969.5 is missing thus ruling out this interpretation). The major band at 960.7 cm^{-1}, however, is not characteristic for ethylene in a CO_2 matrix, indicating that the majority of the ethylene molecules are not residing separately in an argon or CO_2 phase. They appear to occupy interfacial sites in between microcrystallites, or in a mixed phase. Thus, the 1:1 mixed matrix exhibits some phase separation but also selective trapping of the two reactants, effectively decreasing the chances for ozone-ethylene adduct formation and consequently of the reaction probability. Indeed, no reaction was observed in the 1:1 Ar/CO_2 mixture. Additional experiments that included only one reactant revealed that the distribution of each reactant among the two phases as determined from the vibrational IR bands, was not affected by the presence of the other. In this mixed matrix, even though a separate CO_2 phase seems to be formed and ν_+/ν_- bands associated with the amorphous phase are present, no indication for a crystallization process could be observed upon heating to 26 K or even to 35 K. It is possible that the cooperative crystallization process is hindered by the presence of the argon impurity.

The ozone bands in the 1:9 Ar/CO_2 mixture indicate that ozone is located primarily in a CO_2 phase. The ethylene spectra are more complicated, indicating that these molecules 'prefer' to reside in a CO_2 phase, though a considerable fraction occupy sites in between the phases, or in a mixed trapping site. Heating the matrix to 26 K, leads to a decrease in ν_+/ν_- band intensity and to the initiation of a reaction (Figure 8).

Thus the results of experiments in Ar/CO_2 mixed matrices agree with the suggested reaction model, showing again that when crystallization is hindered there is no reaction and that the phase transition initiated at 26 K occurs concurrently with the reaction.

5.3 The reaction temperature dependence:

Another support for the close relationship between the crystallization process and the ozonation reaction arises from the difference between the temperature dependence of reaction yield in CO_2 vs. the argon matrices. For the TME:ozone system in an amorphous CO_2 matrix, once the product bands reached a plateau (at 26 K), heating the matrix to higher temperatures did not generate any further product. It appears that the reaction at that low temperature exhausted the reactivity potential of the matrix. In contrast, ozonation of TME in argon displayed a different temperature-time behavior: the product bands reached a plateau at a given temperature with time, as in the CO_2 matrix. However; further temperature rise led to a pronounced increase in product absorption peaks (see figure 4). This pattern is expected for a matrix containing several sites with varying goemetries, resulting with reactant pairs with different activation energies. The different activation barriers may relate to orientational changes within the trapping sites. Since in the amorphous CO_2 matrix this pattern is not found, site distinction does not affect the reaction rate, as expected if the main effect is due to long range phase changes.

In particular, extensive product formation was observed at 40 K, a temperature at which the matrix is still intact, though much more flexible than at 35 K. It is clear that the 'softening' of the matrix is related to the onset of a rapid reaction. The simplest interpretation is that TME and ozone are able to approach each other at this temperature by diffusion and being free from spatial restrictions, proceed to react. This pattern was found also for ethylene [5] at the same temperature, in spite of the large difference between the high temperature activation energies of these two reactions (Table 1).

The codeposition experiment, in which TME and ethylene were deposited together in an amorphous CO_2 matrix, provides further insight to the reaction mechanism. It was found that the onset temperature of the products appearance was practically identical for the two olefins. The rate of TME ozonation was about 30 times faster than that of ethylene, while the rate constant were practically the same (Section 3.4). The most plausible explanation of this result is that the concentration of TME-ozone pairs in the matrix is much larger than that of the ethylene-ozone pairs. This would be the expected trend in thermodynamic equilibrium, as the van der Waals binding energy of ozone to TME is expected to be much larger than that of ethylene. This is due to the larger size of TME, and also to the increased electron density on the double bond, acting to better bind to the electrophilic ozone.

10

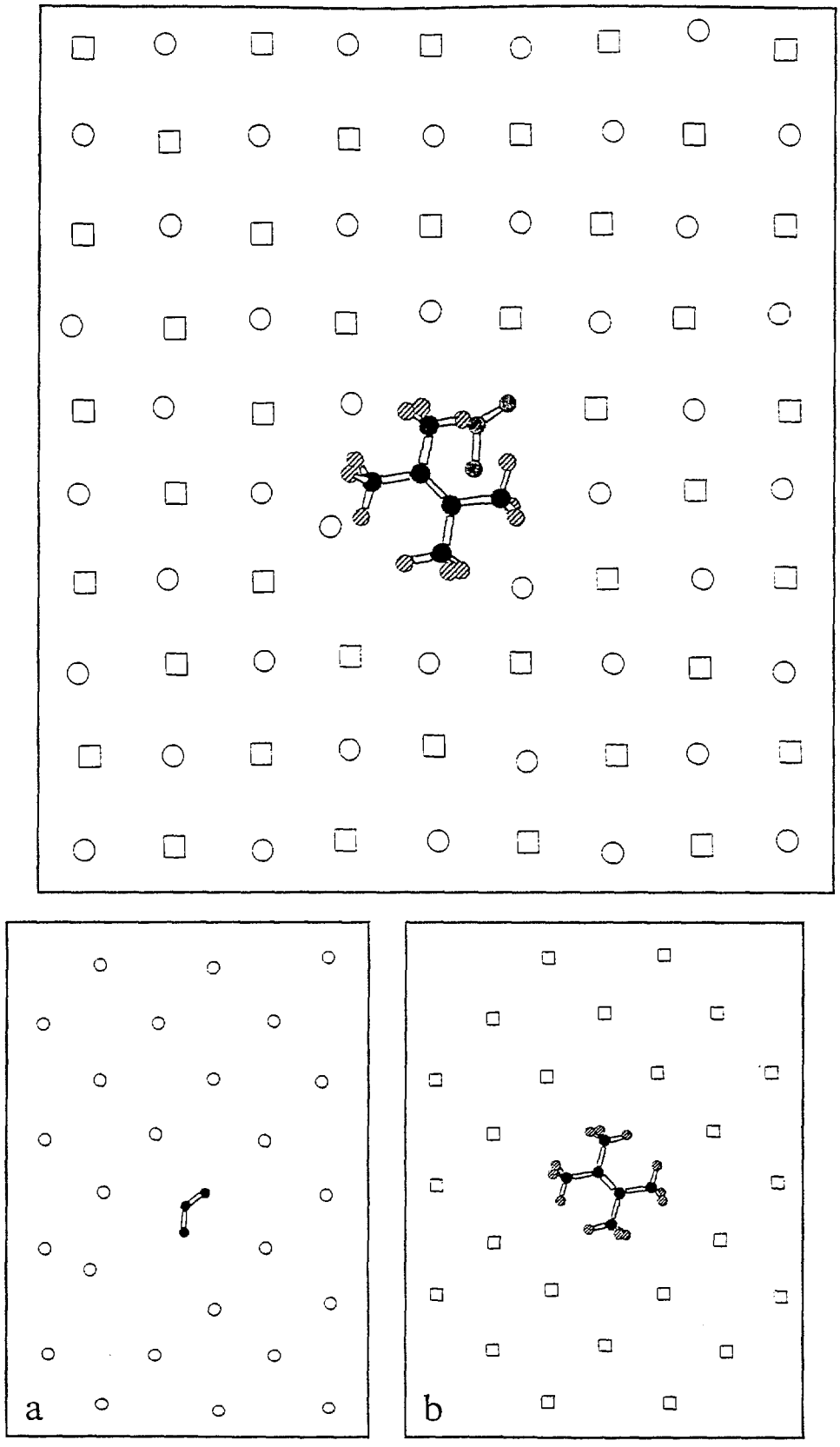

Figure 10. MD calculated, six substitution site of the ozone - TME pair, in an argon matrix. The figure displays two 100 planes. The argon atoms constituting the top 100 argon plane are represented by open circles and the argon atoms constituting the lower 100 argon plane by open squares. Carbon atoms are black, ozone atoms gray and hydrogen atoms are marked by black and white stripes. Figure 10a shows the upper 100 plane and figure 10b shows the lower 100 plane.

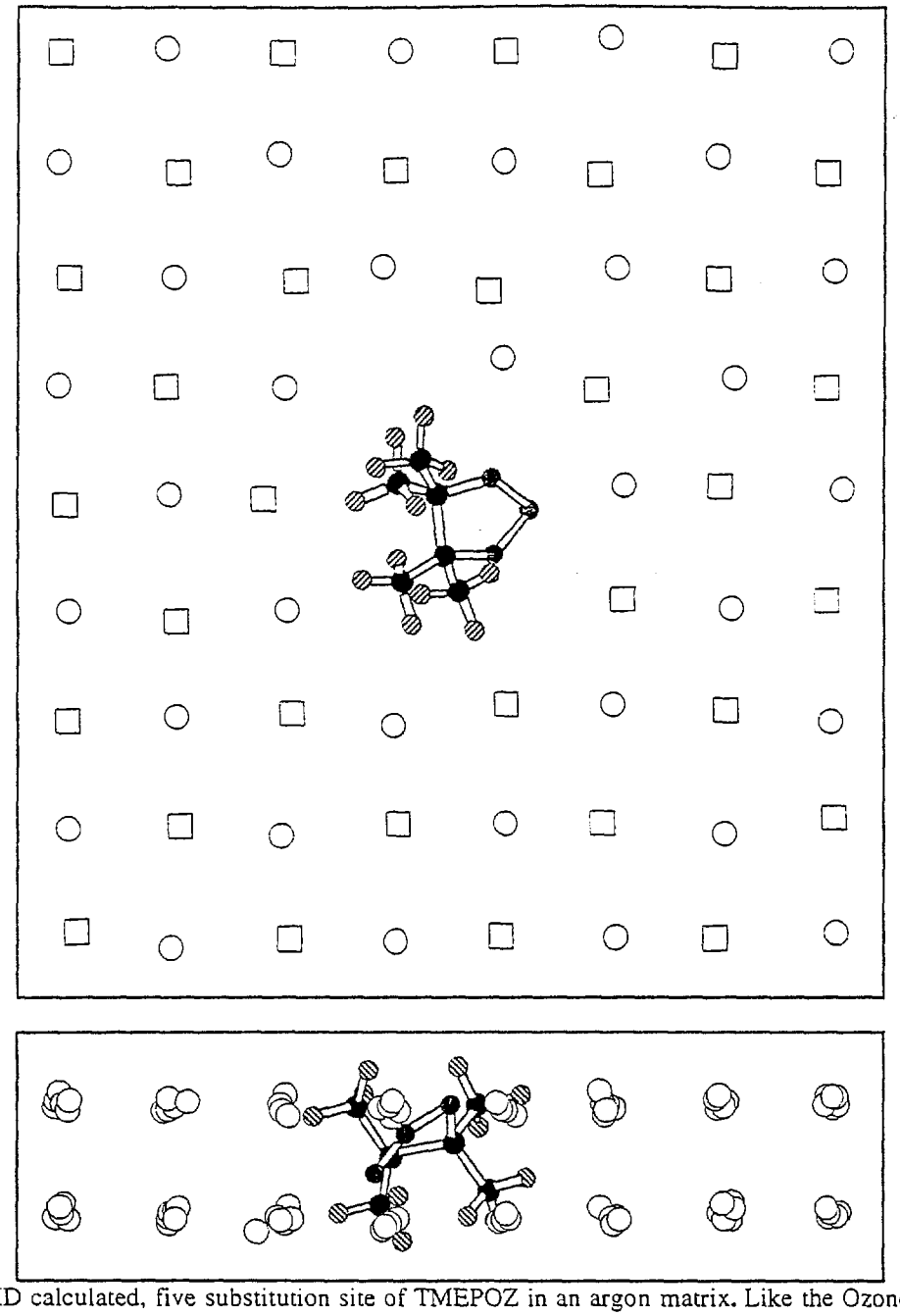

Figure 11. MD calculated, five substitution site of TMEPOZ in an argon matrix. Like the Ozone - TME pair, the ozonide is also trapped in two adjacent 100 planes. Two argon atoms are missing in the upper 100 plane and three in the lower 100 plane. The bottom part shows a side view of the same site.

6. MOLECULAR DYNAMICS SIMULATIONS

In an attempt to rationalize the reactivity pattern observed for TME in argon, molecular dynamics (MD) simulations [31] of the trapping sites of TME/ozone pairs and of the product TMEPOZ were carried out. Such simulations [5] indicated that ethylene ozonation in an argon matrix is unlikely: all calculated trapping sites containing an ethylene-ozone pair were found to be unable to accommodate EPOZ. Rather, the calculated site of EPOZ was larger in volume than that of any site of ethylene-ozone pair, predicting that no reaction will take place in argon, as found experimentally. In the present simulations, as in the case of the ethylene/ozone pair, the molecules were treated as rigid bodies, using the quantum chemical calculated structure (Section 4.1.2).

The TME/ozone pair was found to be trapped predominantly in five or six substitution sites. In both the argon atoms were replaced in two adjacent 100 planes. As an example, **Figure 10** shows the MD calculated six substitutional site of the TME/ozone pair in an argon matrix. For clarity, Figure 10a shows one 100 plane from which argon atoms are replaced, and Figure 10b the adjacent one. In the former the ozone molecule is seen to replace two argon atoms and one more argon atom is considerably displaced from its original position. In the other, TME replaces four argon atoms.

The ozonation product TMEPOZ was also calculated to occupy either a five or a six substitution sites, again in two adjacent 100 planes. **Figure 11** shows a MD calculated, five substitution site of the TMEPOZ in an argon matrix. Like the TME/ozone pair, the ozonide is also found in two adjacent 100 planes. Two argon atoms are replaced in one 100 plane and three in the other (figure 11). The bottom part of Figure 11 shows a side view of the MD calculated five substitution site of the TMEPOZ.

Comparison of the calculated site structures of the ozone-TME pair with that of the TMEPOZ shows the TME/ozone sites can easily accommodate the product. In sharp contrast to the ethylene/ozone case, there is no obvious spatial hindrance for the reaction of the ozone and TME pair to form the TMEPOZ in an argon matrix. For example the 6-substitution trapping site of the ozone-TME adduct shown in figure 10 is similar in structure to that of the product's, the TMEPOZ site, shown in figure 11. Moreover the site occupied by the ozonide product is smaller implying that there is enough room in the pair site to allow it to form the ozonide product.

For a reaction to be feasible the ozone and TME molecules must be situated in the proper relative orientation that allows the formation of the product TMEPOZ. Many of the pair's calculated sites do not conform with this criteria, but some do (such one site was shown above). Thus, the simulation predicts that some of the ozone-TME adduct sites will allow a reaction in argon, as found experimentally. Moreover, since the trapping sites of the ozone-TME pair are found to be fairly spacious, the temperature/time pattern discussed in Section 5.3 can be qualitatively accounted for. At low temperatures, only those pairs that are found in a favorable orientation will react. Other trapping sites remain inert, even though they contain the two reactants in close proximity. Raising the temperature induces thermal motion that leads to the proper orientation for reaction in additional sites.

7. SUMMARY

It is found that the ozonation of both TME and 1-Hexene takes place at the low temperature of 26 K in an amorphous CO_2 matrix. (In line with our previous findings for ethylene). The pseudo first order rate constant for ethylene and TME is essentially the same, even though the high temperature activation energy for ethylene is much larger than for TME. 26 K is the temperature at which amorphous CO_2 undergoes a phase transition to a crystalline phase; it is suggested that this macroscopic cooperative change allows the re-orientation of the reactants, and thus enables their reaction. In a crystalline argon matrix, ethylene and 1-hexene remain inactive up to the softening temperature of this crystalline matrix. This was previously found to be consistent with molecular dynamics (MD) simulations on ethylene/ozone deposition in argon [5] - the two reactants were found to be trapped in a configuration that does not enable the formation of the primary ozonide. In contrast, MD simulations of the TME/ozone pair show that deposition in argon leads to trapping sites capable of supporting the reaction. The temperature dependence of the reaction rate is interpreted as showing that intra-site reorientation is needed for the reaction to proceed. An attempt to overcome the mechanical fragility of the amorphous CO_2 matrix through the use of argon/CO_2 mixed matrices showed that a reaction commenced only when CO_2 percentage was 90%. The absence of reaction in the mixed matrices (argon percentage being larger than 10%) is attributed to the absence of CO_2 crystallization under these conditions and to limited number of reactant pairs formed due to phase separation.

It is concluded, that in both argon and CO_2 matrices, the addition of ozone to the olefins takes place even at very low temperatures, provided the pairs can attain the necessary relative orientation. This implies that the high temperature activation energy, which was reported to be as high as 5 kcal/mol in the case of ethylene, is irrelevant to the matrix studies.

Quantum chemical calculations of the structures and IR spectra of the primary and secondary ozonides of 1-hexene and TME are reported. The calculated spectra are in reasonable agreement with the experimental ones. The calculated structures were used in the MD simulations of the trapping in solid argon.

ACKNOWLEDGMENTS

This research was supported under Grant No. HRN-2078, C12-223, US-Israel Cooperative Development Research Program, Office of the Science Advisor, US Agency for International Development. The Farkas Center is supported by Minerva mbH, Munich. We thank Prof. K. Griesbaum for useful correspondence and for reporting some of his data prior to publication.

REFERENCES

1. R. Criegee, Rec. Chem. Prog. 18 111 (1957).
2. R. Kuczkowski, Chem. Soc. Rev. 79 (1992).
3. D. Cremer, E. Kraka, M.L. McKee and T.P. Radhakrishnan, Chem. Phys. Lett. 187, 491 (1991).
4. R. Ponec, G. Yuzhakov, Y. Haas and U. Samuni, J. Org. Chem. 62, 2757-2762 (1997).
5. U. Samuni, R. Fraenkel, Y. Haas and R. Fajgar and J. Pola, J. Am. Chem. Soc. 118, 3687 (1996).
6. E. Knözinger, W. Schuller and W. Langel, J. Phys. Chem. 97, 927 (1993).
7. W. B. DeMore, Int. J. Chem. Kin. 1, 209 (1969).

13

8. K. H. Becker, U. Schurath and H. Seitz, Int. J. Chem. Kin. 6, 725 (1974).
9. R. Atkinson and W. P. L. Carter, Chemical Reviews 84, 437-470 (1984).
10. L. A. Hull, I. C. Hisatsune and J. Heicklen, J. Am. Chem. Soc. 94, 4856-4864 (1972).
11. B. Nelander and L. Nord J. Am. Chem. Soc. 101, 3769 (1979).
12. K.A. Singmaster and G.C. Pimentel, J. Phys. Chem. 94, 5226 (1990).
13. H. Niki, P. D. Maker, C. M. Savage, L. P. Breitenbach and M. D. Hurley J. Phys. Chem. 91, 941-946 (1987).
14. R. I. Martinez and J. T. Herron J. Phys. Chem. 91, 946-953 (1987).
15. D. Grosjean, E. Grosjean and E. L. Williams II, Envi. Sci. Tech. 28, 186-196 (1994).
16. R. Fajgar, J. Vitek, Y. Haas and J. Pola, To be published.
17. S.D. Razumovskii and L.V. Berezova, Izvest. Akad. Nauk S.S.S. R., Sov. Chim. 1, 207 (1968).
18. N. I. Boldenkov and S. D. Razumovskii, Khim. Prom-st. 2, 100-103 (1977).
19. B. Mile and G.W. Morris and W.G. Alcock, J.C.S. Perkin II, 1644 (1979).
20. P.S. Bailey Ozonation in Organic Chemsitry, Academic Press, New York, 1978 Vol. I.
21. P.S. Bailey Chem. Rev. 58, 925 (1958).
22. K. Griesbaum, W. Volpp and R. Greinert J. Am. Chem. Soc. 107, 5309 (1985).
23. K. Griesbaum, W. Volpp and R. Greinert, H.-J. Greunig, J. Schmid and H. Henke J. Org. Chem. 54, 383-389 (1989); and private correspondence.
24. M. Falk and P. F. Seto, Can. J. Spectrosc. 31 134 (1986).
25. M. Falk, Can. J. Chem. Phys. 86 560 (1987).
26. H. L. Löwen, K. D. Bier, H. J. Jodl, A. Löwenschuss and A. Givan, J. Chem. Phys. 90 5309 (1989).
27. W. Schulze and H. Abe, Chem. Phys. 52, 381-388 (1980).
28. M. J. Frisch, G. W. Trucks, H. B. Schlegel, P. M. W. Gill, B. G. Johnson, M. A. Robb, J. R. Cheeseman, T. Keith, G. A. Petersson, J. A. Montgomery, K. Raghavachari, M. A. Al-Laham, V. G. Zakrzewski, J. V. Ortiz, J. B. Foresman, J. Cioslowski, B. B. Stefanov, A. Nanayakkara, M. Challacombe, C. Y. Peng, P. Y. Ayala, W. Chen, M. W. Wong, J. L. Andres, E. S. Replogle, R. Gomperts, R. L. Martin, D. J. Fox, J. S. Binkley, D. J. Defrees, J. Baker, J. P. Stewart, M. Head-Gordon, C. Gonzalez, and J. A. Pople, Gaussian 94, Revision D.4, Gaussian, Inc., Pittsburgh PA, 1995.
29. W. J. Hehre, R. Ditchfield and J. A. Pople, J. Chem. Phys. 56 2257 (1972).
30. M. W. Wong, Chem. Phys. Lett. 256, 391-399 (1996).
31. R. Fraenkel and Y. Haas, Chem. Phys., 186 185 (1994).
32. M. P. Allen and D. J. Tildesley, Computer Simulations of Liquids (Oxford University, New York, 1987).
33. J. Z. Gillies, C. W. Gillies, R. D. Suenram and F. J. Lovas, J. Am. Chem. Soc., 110 7991 (1988).
34. U. Samuni and Y. Haas, Spectrochim. Acta. Part A 52, 1479-1492 (1996).
35. C. W. Gillies and R. L. Kuczkowski, J. Am. Chem. Soc., 94 6337, 7609 (1972).
36. R. Latimer, R. L. Kuczkowski and C. W. Gillies, J. Am. Chem. Soc., 96 348 (1974).
37. C. S. Murthy, S. F. O'Shea and I. R. McDonald, Mol. Phys. 50, 531 (1983).
38. D. Lucas, Ph.D. Dissertation, University of California, Berkeley, California, 1976.
39. G. C. Pimentel, Ber. Bunsenges. Phys. Chem. 82, 2-6 (1978).
40. B. Nelander and L. Nord, Tetrahedron Lett., 32 2821 (1977).
41. L. Andrews and C. K. Kohlmiller, J. Phys. Chem. 86, 4548-4557 (1982).
42. CRC Handbook of Chemistry and Physics, 60th edition, Editors R.C. Weast and M. J. Astle, 1979.
43. W. Press, B. Janik and H. Grimm, Z. Phys. B- Condensed Matter 49, 9-16 (1982).
44. W. Langel, A. Becker, H.-W. Fleger and E. Knozinger, J. Mol. Str. 297, 407-413 (1993).
45. W. Langel, H.-W. Fleger, E. Knozinger and W. Schuller, Ber. Bunsenges. Phys. Chem. 99, 940-950 (1995).
46. S. Nose and M. L. Klein, Can. J. Phys. 60, 1365-1370, (1982).

74